Soil Moisture Dynamics and the Effects on Initiation of Aeolian Sand Transport

MSc Thesis Earth Surface and Water – Coastal Dynamics and Fluvial Systems

Student: J.T. Tuijnman (5765676)
1st supervisor: prof. dr. B.G Ruessink
2nd supervisor: dr. J.J.A Donker

(Final Version, Dec 20, 2018)

Universiteit Utrecht

Abstract

Aeolian sediment transport is the most important source of sediment supply for the growth of fore-dunes, which provides an important societal function by protecting the hinterland from flooding. Furthermore, delivery of aeolian sand to the hinterland creates new habitat which pioneer species can colonize, enhancing biodiversity in coastal dune areas. Soil moisture is recognized as important aeolian sediment transport controlling factor by increasing the shear velocity threshold needed to mobilize sediment and by reducing the aeolian transport rate over a wet surface under certain wind (<12 m/s) conditions. In this study, results of detailed measurements on spatial and temporal soil moisture dynamics conducted with a Delta-T Theta probe on a wave-dominated beach in Egmond aan Zee, the Netherlands are presented. Moisture measurements along a well transect over the course of one month focus on cross-shore spatial (x = 110 *m*) variability in relation to the groundwater level below the surface of the beach. Furthermore, the cross-shore distribution of moisture content is discussed in terms of tidal and morphological induced variation and as potential aeolian transport reducing factor. Piezometric head measurements reveal tidal induced oscillations of the phreatic surface and showed a correlation with the soil moisture variation at the surface of the beach by a fitted retention curve. Observations of a seepage face during and after a storm surge reveal that the potential area available for aeolian transport is strongly reduced, because shoreward of the seepage face exit point the aeolian saltation system is closed and wet moisture conditions remain after the surge has passed. Furthermore, field based observations of soil moisture and wind speed near the threshold of aeolian transport revealed an increasing threshold of wind speed with moisture content. These observations do not match with predictions using a moisture corrected threshold value based on wind shear. The shifting of a moisture dependent threshold region could be used to fine-tune process based models that use the fetch-effect to calculate a downwind increase in transport. Incorporation of this threshold region implies defining a spatial and temporal varying contour of equal (threshold) moisture content, landward of this zone the critical fetch distance is reached and aeolian transport starts.

Table of Contents

1. Introduction

Windblown sand transport is the most important source of sediment supply for the development of dunes on sandy beaches (Davidson-Arnott et al*.,* 2005) dunes provide important societal and ecological functions; they provide natural protection against marine flooding, especially when the hinterland is densely populated and low lying as in the Netherlands (deWinter *et al*., 2015). Furthermore, dunes possess high ecological value, that is essential to preserve in order to maintain biodiversity associated with the colonization of pioneer species (Everard *et al.,* 2010). It is therefore important to understand processes that influence the growth and erosion of dunes. This knowledge may help to develop predictive models that calculate the rate of growth of the foredunes by estimating the flux of sand from the beach which in turn helps establishing a closed form sediment budget of the coastal area (Bauer and Davidson-Arnott, 2003).

However, limited knowledge of feedback mechanisms between controlling factors of the nearshore aeolian system confound our ability to model and predict sand transport (Davidson-Arnott and Law, 1990; Bauer et al., 2009; Schmutz and Namikas 2018). Properties of the sand surface (morphology, roughness, grain size, moisture content, vegetation etc.) and the wind field (wind speed, direction, unsteadiness, boundary layer development, flow compression) often interact in unknown and complex ways to alter the equilibrium transport conditions as adapted in most physical and empirical based models (Bauer et al. 2009). Therefore, potential transport as estimated by conventional aeolian models is far from indicative for long-term predictions of sediment supply from the (intertidal) beach to the fore-dunes (Arens, 1991)

The focus of this study lies on the effect of soil moisture content; which is widely acknowledged as key parameter in aeolian environments that increases the shear velocity threshold needed to mobilize sediment (Wiggs *et al.*, 2004; Bauer *et al*., 2009; Nield *et al*., 2011). All other controlling factors being equal, less sand is transported over a moist surface compared to a dry surface because the entrainment threshold is increased via interparticle cohesion associated with the presence of moisture (Bauer *et al.,* 2009; Namikas *et al.,* 2010).

An important aspect not taken into account in most predictive aeolian studies is the presence of beach soil moisture content, let alone it's temporal and spatial variability (Wiggs *et al.*, 2004; Namikas *et al.,* 2010*;* Ellis and Sherman*,* 2013). In coastal areas, the absence of this factor is suspected to contribute to the yet unresolved prediction of sediment transport (Delgado-Fernandez, 2010; de Vries *et al.,* 2014). Variability of the surface moisture distribution arises on different time and spatial scales (Namikas, 2010). Firstly, on a semi-diurnal scale due to inundation of the beach associated with the tides. Furthermore, a number of studies confirm that tidal induced oscillations of the groundwater table play a role in governing the distribution of the surface moisture (McKenna Neuman and Langston, 2006; Oblinger and Anthony, 2008; Darke and McKenna Neuman 2008; Poortinga *et al.,* 2015).

On time scales of days to weeks the effect of morphological evolution may alter the surface moisture distribution. Intertidal sandbars migrate landward during quiet wave conditions due to gradients in acceleration skewness and currents associated with wave cell circulation (Hoefel and Elgar, 2003). In contrast, during storms the intertidal sandbars or parts of the beach face are erode due to large gradients in the undertow currents and sand concentrations (Hoefel and Elgar, 2003). Next to modifying the surface moisture distribution other characteristics of the surface (e.g grainsize sorting and distribution De Vries *et al.*, 2014) important for aeolian transport are altered by the morphologocial evulation.

Together, the evolution of the morphology and groundwater oscillations associated with the tides may alter the spatial and temporal organization of the surface moisture content, which in turn impacts the conditions for aeolian transport. Although, there are numerous studies that indicate the importance of surface moisture in modifying the dynamics of the aeolian system, only a few actually report field data and describe the spatial and temporal variation of this control (Wiggs *et al*., 2003; Bauer *et al*., 2009; Namikas *et al.,* 2010 and others). It is therefore essential to deploy additional surface moisture measurements in the field to gain an improved understanding of this important aeolian sand-transport control.

The overarching aim of this study is to quantify temporal and spatial variability in surface moisture content and investigate moisture dependent entrainment thresholds on a sandy beach in Egmond aan Zee, the Netherlands. The surface moisture variability is investigated on a spatial scale characterised by cross-shore distance of the intertidal beach (x = 120 m). Temporal scales of variability that are investigated are associated with the tides and morphological evolution of the beach (hours to weeks).

Structure of the thesis is as follows; starting with a rather broad literature review (chapter 2) where physics and controls on the surface moisture distribution and entrainment thresholds are reported based on previously conducted research. Followed by the methods section (chapter 3), where the framework of this study (Aeolex II), a fieldsite description and the experiment design are spelled-out. Subsequently results of the field experiments are given in chapter 4 which are discussed in the next chapter 5. Ultimately, the conclusions of the study are given in chapter 6.

2. Literature Review

The importance of soil moisture in aeolian studies is widely recognized, cohesive forces associated with the presence of moisture can act as transport influencing and entrainment threshold increasing factor (Namikas and Sherman, 1995; Artherton, Baird and Wiggs, 2001; Davidson-Arnott *et al*, 2008; Namikas *et al.* 2010). Soil moisture content (w) of a beach is controlled by a number of processes that can be characterised in terms of a budget (insert of Figure 2-1), including sources, sinks and storage (Namikas *et al*., 2010). Input (or output) of moisture to the system can be divided in marine, atmospheric and groundwater sources (or sinks) (Namikas *et al*., 2010). Spatial and temporal variability in soil moisture content emerges due to the unsteady and non-uniform nature of the controlling processes and their interactions. The amount of potential storage (the water that can be hold in the intergranular pore spaces) is controlled by the sediment texture of the beach and derivative parameters like porosity, hydraulic conductivity and field capacity (Fitts, 2002; Namikas *et al*., 2010). Soil moisture (or surface moisture content as used throughout this study) is almost always expressed as a percent of weight (or sometimes of volume) of a sediment sample (equation 2.1) (Namikas and Sherman, 1995).

$$w = \frac{(w_s - w_d)}{w_d} \cdot 100\% \qquad (2.1)$$

Where w is the surface moisture content (%), w_s is the total sample weight (g) and w_d (g) the dry sample weight.

Two main forces are responsible for the increased interparticle attraction imposed by the presence of moisture (Wiggs *et al.*, 2004). Surface tension (in γ in N/m) imparts a cohesive force that binds grains together when moisture is present in the pore spaces between the grains. It is the surface of water that acts as an elastic membrane around the grain as water molecules stretch and are attracted to each other (Namikas and Sherman, 1995). In addition, water wedges form at the contact points of grains as a result of capillary forces (McKenna Neumann and Nickling, 1989). These two forces work together to retain water in the sediment matrix, against the action of gravitational drainage and thereby increase the resistance of particles at the surface of the beach to aeolian entrainment (Wiggs *et al.,* 2004).

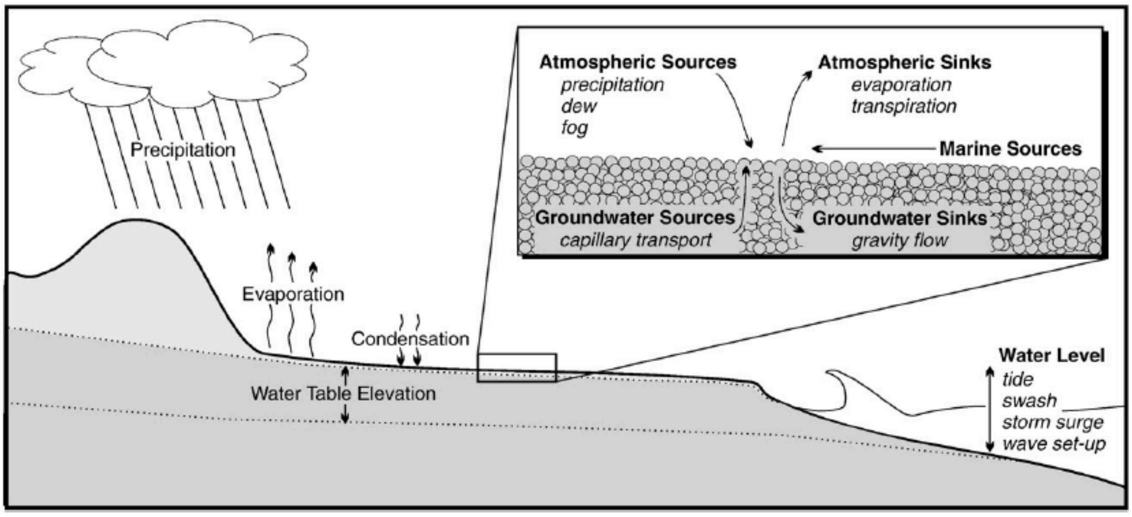

Figure 2-1 The soil moisture budget, overview of sinks and sources. Moisture content at any given time and location is the net sum of in and outputs from the various processes. (adapted from Namikas et al. 2010). With illustrative depth of the groundwater watertable during both low and high water are indicated.

2.1 Marine Influences

Marine inputs that influence the soil moisture content generally enter via the intertidal and swash zones of the beach due to sea level variations; on a periodic basis (via tides and waves) and on a less regular basis (via wave spray and storm surge) (Bauer *et al.*, 2009; Namikas *et al.*, 2010). Large part of studying and understanding periodic sea level variations includes decomposing time-serie signals. Because sea level variations compromise a set of components with different phases and amplitudes that can be distinguished from another (Sánchez-Úbeda *et al.*, 2016).

All components that make for the sea-level variations are expected to generate a cross-shore gradient in the spatial distribution of the soil moisture content of the beach (Namikas *et al.,* 2010). Emitting subsurface and atmospheric inputs and outputs from the budget and solely considering marine processes, a moisture distribution with saturated conditions due to wave run-up infiltration at the seaward part of the beach and dry conditions landward from this point are conceptualised. Further simplifying, and assuming alongshore uniformity but including the periodic semidiurnal variability of rising and falling tides generates a picture of a cross-shore shifting saturated zone with periodicity of the wind, swell and infragravity waves superimposed on the tidal oscillations.

The two different moisture zones obtained by simplifying the budget in this manner are thus; 1) a dry zone bounded by the landward dune-toe and 2) the saturated zone that is bounded by the shoreline and wetted by wave run-up infiltration and largely controlled by periodicity waves at infragravity frequencies (if waves are considered present). Other components with less periodicity that also affect the shifting of the two moisture zones include storm surge and river discharge.

2.2 Subsurface Influences

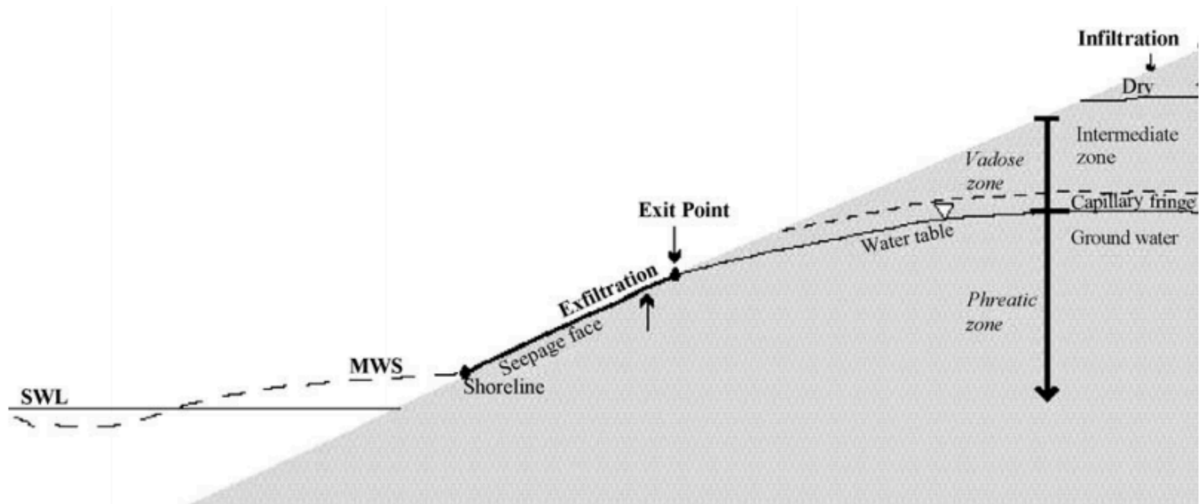

Figure 2-2 After Horn (2002) Illustration of beach groundwater definitions and concepts. In this study, Mean Water Surface (MWS) is used interchangeably with Sea Surface elevation (SSE).

The simplistic and conceptual sharp boundary between saturated and dry beach becomes more complicated when groundwater influences are added to the budget (Figure 2-2) which makes for the presence of a third shifting moisture zone. This third, intermediate zone is characterised by neither dry or saturated conditions, the pores of the intergranular sediment matrix are partly filled with water and air. This zone exists because of infiltration of water that was exposed at the surface of the beach (due to tidal inundation and wave run-up or rainfall) which percolates down to the groundwater table such that the beach surface may partly dry-up again. In contrast, subsurface water may reach the surface again via capillary forces in the intermediate zone (vadose zone) depending on the depth of the groundwater table (phreatic surface) below the surface and sediment texture.

In coastal hydrology, the beach is usually threated as an unconfined aquifer, with oscillating pressure heads caused by the tides driving subsurface water flow described by Darcy's law (equation 1) where the upper boundary of groundwater flow is defined by the watertable (figure 2-2) (Fitts, 2002; Horn, 2002). Subsurface water in granular materials (like a sandy beach) exists in an interconnected network of pores between the solid mineral grains. The intergranular porosity (*n*) is a dimensionless property defined as the fraction of the material volume that is pore space (Fitts, 2002) and determines the amount of water in the subsurface. The distribution of the grainsize is a key parameter that controls the porosity and thus the amount of water that is present and how easily water is transmitted through the sediment matrix (Fitts, 2002). Darcy's law reads

$$Q_s = -K_s \frac{dh}{ds} A \qquad \text{(2.2) Darcy's law}$$

Where Q_s is discharge in the cross-shore s direction (positive onshore, negative offshore), K_s the hydraulic conductivity in the s direction, dh/ds denote the head difference over distance s and A the cross-sectional area of the medium where flow is considered.

The major part of studies done on beach groundwater behaviour focused on the tide-induced fluctuations (Horn 2002). Findings show that the elevation of the groundwater table on beaches is known to oscillate at frequencies associated with the tides (Lanyon et al., 1982; Li et al., 1997). Especially in meso- and macrotidal environments the influence of the tide is dominating over other factors (Gourlay 1992; Li *et al*., 1997). Other factors include groundwater table oscillations due to the breaking of waves with resulting set-up and wave run-up infiltration (Gourley, 1992; Nielsen and Kang, 1996 Turner *et al*., 1997).

The beach is sometimes referred to as a low-pass filter; higher frequency oscillations tend to be filtered out of the signal when moving landward (Lanyon *et al.,* 1982). Raubenheimer et al. (1999) found that the semi-diurnal and diurnal signal are almost completely damped 100m landward of the mean shoreline location, where harmonics with longer periods (spring-neap at ≈ 14 days) attenuate less. Pollock *et al*. (1971) compared influence of spring and neap tidal cycles on groundwater and found that the upper beach drained more completely during neap than at spring tides. Furthermore, landward amplitudes of the watertable fluctuations decrease, the phase lag increases and the signal becomes more asymmetrical and skewed in time (Raubenheimer et al., 1999).

Other than marine factors, recharge from the backshore (the dunes) and characteristics of the beach material that determine the hydraulic conductivity such as grainsize, sediment shape, sorting and porosity control the elevation of the watertable (Gourley, 1992). Furthermore, wave setup and runup at the beach face cause infiltration and hence cause super-elevation of the watertable, resulting in a beach watertable that is in general higher than mean sea level (Turner et al., 1995). This excess elevation of the watertable (or overheight or super-elevation) increases with distance from the shore and decreasing hydraulic conductivity (Turner et al., 1995; Raubenheimer *et al.,* 1999). Observations of the watertable behaviour show thus that the watertable is generally not flat and that its slope and the direction of the slope also changes with the tide. Lanyon et al. (1982) found that during a rising tide the water table slopes landward and during falling tide the water table slopes seaward.

The periodic rise and fall of the tide and imposed wave conditions result in a variation of the watertable elevation, of which the time-series signal is asymmetrical, due to differences in drainage and infiltration speed. The watertable rises abruptly and drops off more slowly because vertical infiltration at high tide is easier compared to lateral draining at low tide caused by difference in area of the beach that is available for infiltration and exfiltration during wetting and drying (Pollock and Hummon *et al.,* 1971; Nielsen 1990; Gourley 1992, Turner *et al.,* 1995). It is expected that this trend (of slow drying and fast wetting) is also reflected in temporal soil moisture variations at the surface of the beach.

2.3 Seepage

An important phenomenon that controls the beach soil moisture content and arises due to the interplay between tides and groundwater is the occurrence of seepage faces (illustrated in Figure 2-2). The visual occurrence is characterised by a wet and glassy beach surface, where the sediment matrix is fully saturated with water and exfiltration happens via the beach surface (Horn, 2002). The geometry and timing of seepage faces are of importance in aeolian studies because it reduces the potential area of the beach that is available for aeolian transport by saturating the beach surface. It should however be noted that the visual occurrence of the exit point lays some distance landward of the exit point depending on the thickness of the capillary fringe.

Seepage faces usually develop during a falling tide, between the shoreline and at the intersection of the beach profile and the groundwater table (the exit point, figure 2-2). This usually happens when the tide falls faster than the beach drains (Nielsen 1990; Raubenheimer et al. 1999; Horn, 2002). After decoupling of the watertable and the tide, the exit point is independent of the shoreline location. The presence of a seepage face is next to the relative speed between the falling tide and watertable also dependent on the morphology of the beach. A seepage face resembles the groundwater table because it is also at atmospheric pressure however, the shape of the seepage face is distinguished from the watertable since the shape is determined by the beach topography (Horn, 2002).

Next to the seepage face as shown figure 2-2 which continues from the exit point to the shoreline a second type of seepage face that is not depicted in figure 2-2 can be present in bar –trough systems. In such cases the topographic variations associated with bar- trough couplets make for a saturated trough intersecting the bar and intertidal beach (Oblinger and Anthony, 2008).

2.4 Unsaturated Zone

Omitting atmospheric sources and sinks and solely looking at the rising and falling groundwater table due to the tides, the surface moisture content of the beach is augmented by upward water flow from the saturated zone and decreased by a downward flow. When sediments are not completely saturated the wetting and draining of the beach surface can happen by water flow through the unsaturated zone where pore spaces are filled by a combination of air and water. At low pressures, present during a water table far below surface, the water content in the pore spaces is known to remain almost constant with further increase in suction (right side of figure 2-3). After gravitational drainage, the remaining water forms a thin film around the sediment minerals; tightly hold together by forces of mutual attraction between water molecules and sediment minerals (Fitts, 2002). This value of moisture is known as the field capacity and can be determined with a soil water retention curve for a specific sediment which describes the water content as function of suction (Leonh and Rahardi, 1997).

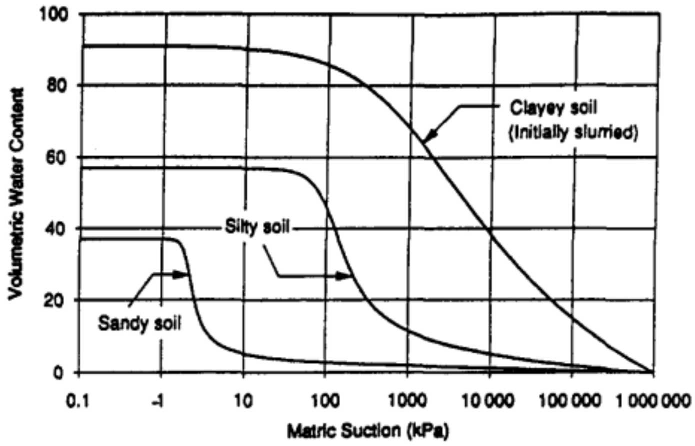

Figure 2-3 Soil-water characteristic curves for sandy, silty and clayey soil. After Leong and Rahardj (1997)

The pore water pressure P in the unsaturated zone is sub-atmospheric due to forces of attraction between the matrix and water molecules (Hillel, 1998; Fitts, 2002; Horn, 2002). The water is attracted to and stretched over the sediment surface. The subatmospheric pressure, or matric suction can result in a negative pressure potential which constitutes a moving force on the water and makes for the capillary fringe to develop above the water table. The capillary fringe is the area where the sediment is still saturated but the pore water pressures are sub-atmospheric due to matric suction (Figure 2-4) (Fitts, 2002; Horn, 2002). As the gravimetric water content decreases the suction forces become increasingly more important compared to other forces driving water flow (Hillel, 1998).

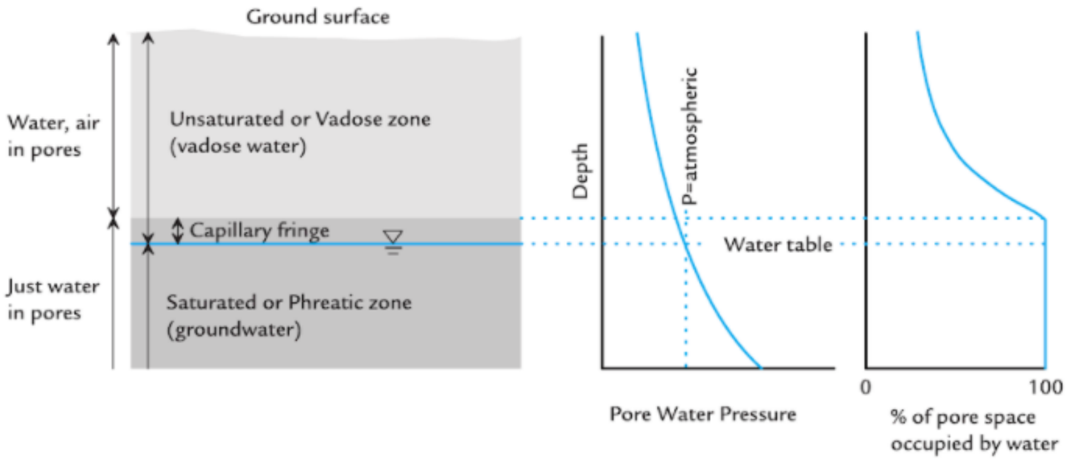

Figure 2-4 Vertical cross-section illustrating terms to describe subsurface water (left), depth as a function of pore water pressure (middle) and volumetric water content (right) after Fitts (2002).

The surface area where water contacts and is attracted to the sediment, increases as grainsize drops and thus the negative pressure generated with this attraction develops (more negative) with decreasing grainsize (Hillel, 1998). The thickness of the capillary fringe therefore depends grainsize of the sediment; fine grained sediments remain saturated by capillary forces to lower pressures compared to coarse grained sediments (figure 2-3). Non-uniformities in suction cause water to flow, in such cases a suction gradients exists. Water will spontaneously flow from areas where suction is lower to where suction is higher.

Describing flow in the unsaturated zone is different from the saturated zone because the hydraulic conductivity K is not a material constant as in the saturated zone but altered by the water content (Hillel, 1998; Fitts, 2002; Schmutz and Namikas, 2013). When the soil is saturated all of pores are water filled and act as a conducting medium. When the pores desaturate, they become partly air filled and the conductive part of the medium decreases (Hillel, 1998). This complicates describing and quantifying unsaturated groundwater flow compared to saturated water flow. However, models to predict unsaturated hydraulic conductivity from knowledge of the soil-water characteristic curve and conductivity at saturation have been long developed and used (van Genuchten, 1980). The following expression was proposed by van Genuchten in 1980 (Equation 2.3).

$$\theta = \theta_r + \frac{\theta_s - \theta_r}{[1+|\alpha h|^n]^m} \qquad (2.3)$$

With θ is the soil water content, θ_r is the residual water content, θ_s is the saturated water content, h is the soil water potential, α is a scale parameter inversely proportional to the mean grain diameter and m and n are shape parameters.

For soil moisture dynamics on the beach it is important to investigate how the gradient in moisture content develops under falling and rising groundwater tables (Schmutz and Namikas, 2013). During falling tide the head difference between two arbitrary points (for example halfway upon the beach and located at the shoreline) increases due to a lowering of the water exit point. The gradient of the head potential causes the subsurface water to flow in the direction of the smallest head. During these conditions (a falling watertable associated with a falling tide) larger sub-atmospheric pressures in the capillary fringe develop. At some point, when sufficient negative pressure is applied (further, falling watertable) the largest pores of the medium start to drain water. This happens when the radius of the largest pores is too great to hold the radius of the meniscus of water to balance the negative pressure (Hillel, 1998). In other words; the pressure head at which the first air enters the largest pores (this is referred to as the air-entry value displayed by the convex point on the curves in Figure 2-3). Suction of a falling water table is thus hindered by retention due to capillary forces.

Pollock and Hummon (1971) noted that on a rather coarse-grained beach (660µm) 50% of the pore-water was lost quickly but that it took far longer for the remaining water to percolate down to the groundwater table. It is expected that this effect is greater in more fine-grained beaches due to the larger capillary forces and can be attributed to the dependence of hydraulic conductivity on water content in unsaturated sediments and capillary forces. Conventionally, the dependence of hydraulic conductivity on water content (transient nature) is ignored in beach moisture content studies where steady state conditions independent of the velocity of the watertable fluctuations are assumed. This Implies synchronous variations in soil moisture content with the cyclic movement of water-table fluctuations (Schmutz and Namikas, 2013). However, with bearing the dependence of hydraulic conductivity on water content in mind, the moisture at the surface may lag behind water table oscillations since flow is reduced more, higher above the watertable as moisture content decreases.

Considering this effect in the spatial distribution of moisture content on the beach it seems likely that the time lag due to transient capillary flow increases landward from the shoreline. Due to, both the larger vertical distances that need to be covered with a deeper water table, and the slower capillary flow with lower moisture contents in the vadose zone landward (Schmutz and Namikas, 2013). In addition to the transient nature of capillary flow that causes non-linear behaviour of soil moisture content there is hysteric behaviour of capillary flow that causes a discrepancy between wetting and drying rates of the sediment column that is also important in beach soil moisture studies (Schmutz and Namikas, 2013).

The hysteresis effect can by studied by comparing the water content of the unsaturated zone during a falling and a rising watertable at the same pressure head. The water content can either be observed at the surface or somewhere in the unsaturated water column (Schmutz and Namikas, 2013). If, however, studied at the surface under natural conditions, atmospheric processes may influence the water content rather than capillary flow alone.

During a falling water-table is observed that moisture contents at a certain level in the sediment column remain higher than during a rising water table at the same pressure head (Figure 2-5). In other words, during a draining cycle (falling water-table), the sediment tends to remain wetter until a lower pressure than would be expected at that same pressure during a wetting cycle (rising water table). Considering the hysteresis effect, it is expected that the capillary thickness and vadose zone moisture content is larger during a falling than during a rising tide. It is therefore expected that the beach surface is moisturized by capillary water until a greater water-table depth during a falling than during a rising tide.

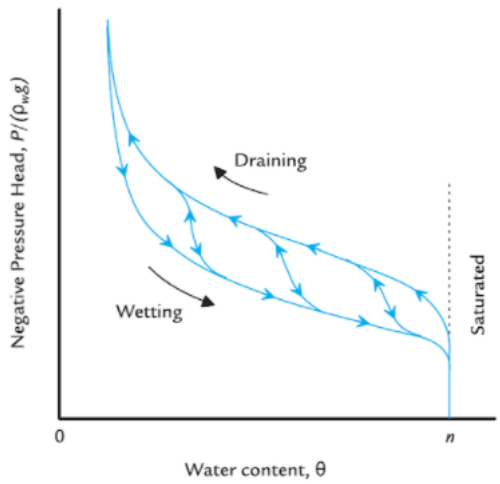

Figure 2-5 Soil water characteristic curves during wetting and draining after Fitts (2002).

2.5 Atmospheric Influences

Precipitation, fog, dew include atmospheric sources for beach soil moisture content. Whereas evaporation and evapotranspiration are atmospheric sinks. In – and outputs are expected of greater spatial uniformity (at least greater than the spatial cross-shore beach scale) than marine or subsurface influences (Namikas *et al*., 2010) and thus only affect the temporal variation of surface moisture content (Zhu, 2007). Drying of the beach surface could occur by evaporation from the bare soil. It is however, expected that moisture is replenished via capillary rise if the groundwater table is close enough to the beach surface (Atherton *et al.,* 2001). In this case the degree of surface drying depends on the balance between moisture gain by capillary rise and moisture loss by evaporation (Atherton *et al.,* 2001). However, the daily evaporation- condensation cycle shifts with a different period than the groundwater variations, therefore the two processes are likely to further increase the spatial and temporal variability in beach soil moisture content (Zhu, 2007).

During atmosphere controlled conditions, when the groundwater table is close enough to the beach surface and evaporative losses are immediately replenished, estimates for free-water evaporation can be used (Dingman, 2015). The Penman equation is widely recognized to give the best results (Dingman, 2015) and is based on the surface energy balance and mass-transfer conditions in which wind speed and relative humidity are major controls. However, as stated above, another stage of evaporation usually occurs on the beach by which evaporative losses are not only controlled by atmospheric conditions but also by unsaturated flow via the soil (Atherton *et al.,* 2001; Dingman, 2015). The shift from atmosphere to soil controlled evaporation can be visually recognised, since the beach surface albedo immediately increases and the surface dries (Dingman, 2015).

In the Netherlands, the royal Dutch meteorological institute (KNMI) uses the Makkink equation (equation 2.4) to calculate reference evaporation, which requires only temperature and incoming solar radiation as input, following Hiemstra and Sluiter (2011).

$$E_{day} = C * \frac{s}{s+\gamma} * \frac{S_{in}}{\lambda * \rho} \quad (2.4)$$

With E is the evaporation (md^{-1}), C a constant taken 0.65, s is the slope of the saturation vapor pressure curve (kPa °C^{-1}) which is modulated by the temperature T (°C) and saturation vapor pressure e_s.

$$s = \frac{7.5*237.3}{(237.3+T_{day})^2} * \ln 10 * e_s \quad (2.4.1)$$

Where e_s equals:

$$e_s = 0.6107 * 10^{\frac{7.5*T_{day}}{237.3+T_{day}}} \quad (2.4.2)$$

The psychometric constant (γ) is related to T_{day}, the mean day temperature by

$$\gamma = 0.0646 + 0.00006 * T_{day} \quad (2.4.3)$$

As well is the heat of vaporization (λ):

$$\lambda = (2501 - 2.375 * T_{day}) * 1000 \quad (2.4.4)$$

2.6 Variability of Beach Surface Moisture Content

A closer look at the soil moisture budget on beaches, shows that controlling mechanisms on the system are numerous and that they work on different spatial and temporal scales and furthermore, mechanisms might influence another. It is to no surprise, that methods to model or simulate soil moisture variability are complex and are largely not yet developed (Schmuts and Namikas, 2013). Nevertheless, a number of studies have tried to identify mechanisms that influence beach soil moisture and shed light on their relative importance in context of aeolian processes.

Conventional methods to study beach surface moisture include the usage of a Delta-T Theta probe that measures impedance (Atherton *et al.,* 2001; Yang and Davidson-Arnott, 2005; Davidson-Arnott *et al.,* 2007; Bauer *et al.,* 2009; Namikas *et al.,* 2010 and others). The probe generates an electrical sinusoidal signal that extends to the soil by means of the four rods. The signal changes with impedance of the soil, which is primarily determined by the water content of the beach since the dielectric constant of water is much higher than of (quartz) sand (Davidson-Arnott *et al.,* 2007). The signal is converted to a voltage of which the magnitude is dependent on the water content and dielectric constant of the sand. Thus, Impedance between the rods reflects the amount of water in the sediment.

Most of the beach surface moisture studies have put effort in using and modifying the effective probe rod length following Yang and Davidson-Arnott (2005). Modifications of the probes are needed in order to obtain a moisture measurement of only the top couple of centimetres of the sediment. Traditionally, the probes were designed to measure in situ water contents of soils for mostly ecological, agricultural or hydrological purposes in the root zone of plants (Legates *et al.,* 2011). Interest in these studies does not necessarily go to measure only the very surface moisture conditions but moisture conditions integrated over some depth.

Modifications to partly overcome this aberration include a reduction of the rod length of the probe, either by using shorter rods as used in this study, or partly encapsulate the longer rods with di-electric foam such that only the tips of the rods are exposed (Davidson-Arnott *et al*., 2007; Edwards and Namikas, 2009). In most studies, the rod length was chosen in the order of 2 cm as a compromise between decrease in precision with further reduction of rod length and measuring as close to the surface as possible.

However, as Edwards *et al.,* (2012) and other threshold studies (Bauer *et al.,* 2009; Cornelis and Gabriels, 2003) indicate, even with a modified rod length, the depth-integrated measurements might not reflect moisture conditions at the surface of the sediment (the upper 2mm or so) since the uppermost surface of the sediment may be characterised by large moisture gradients due to rapid surface drying during aeolian activity, which influences saltation activity (Bauer *et al.,* 2009). Recent efforts to overcome the deviation due to depth integrated measurements include the usage of laser scanning or other remote sensing techniques (Edwards *et al.,* 2012, Smit *et al.,* 2018).

Next to measuring only the very surface of the beach, other advantages of remote sensing techniques include the continuous spatial and temporal coverage of both of topography and soil moisture (Legates *et al.,* 2011*;* Smit *et al.,* 2018). These techniques have been validated in the field as well as in wind tunnel simulations and are based on the principle that light penetrates further into wet compared to dry surfaces. Wet surfaces turn in response darker due to a change in refractive index (Darke and McKenna Neuman, 2008). A combined data assimilation approach using remotely sensed estimates calibrated with in-situ probe or gravimetric moisture measurements to quantify errors and uncertainties seems a promising approach for future surface moisture estimations (Legates *et al.,* 2011).

However, Delta-T theta probes are proven as good devices to measure the soil moisture content of the upper 2 to 1.5 cm of sediment, which can be a good surrogate for the moisture content of the surface of the beach important in aeolian studies (Atherton *et al.,* 2001; Yang and Davidson-Arnott, 2005; Davidson-Arnott *et al.,* 2007; Bauer *et al.,* 2009; Namikas *et al.,* 2010 and others). Furthermore, due to the non-destructive, easy to use and low-budget nature of the sampling method some authors have used, calibrated and modified the Delta-T Theta probes in beach surface moisture studies to quantify spatial and temporal variability. In the following section, methods and results of these studies are described and compared in order to converge to some general findings, contradictions and knowledge gaps on the subject of spatial and temporal soil moisture variability on natural beaches.

Results of Bauer et al., (2009) and Namikas et al., (2010) show that moisture conditions of the upper beach and dune-toe are relatively dry (0-5%) and show little variability. The variability on this beach part is mainly influenced by rainfall, storm surge and changes in relative humidity that varies on a diurnal scale. Namikas et al., (2010) notes that the dry-zone can be a conceptual surrogate for area potentially available for aeolian transport but that the spatio-temporal variation is little but the behaviour is complex and influenced by both tidally induced water table fluctuations and atmospheric parameters. In contrast to Bauer *et al.,* (2009) and Namikas et al., (2010) results of Yang and Davidson-Arnott (2005) and Davidson-Arnott et al., (2007) show larger moisture variability at the dune-toe compared to the mid-beach. The increased moisture content in this area is explained by seepage from the fore-dune slope, sheltering from solar radiation in this area and accumulation of litter and growth of plants that result in a damper beach surface.

Variations in the mid-beach were found more complex to interpret compared to the dry zone. Cool conditions and moist onshore winds together with an extended period of high water table elevations explain increasing wetness of the intermediate zone due capillary transport of water from the phreatic zone to the surface (Namikas et al., 2010). Subsequent drying during the night (with high humidity levels during the day) are linked to gravitational drainage since evaporation is not likely during these conditions. Furthermore Namikas *et al.,* (2010) notes a continued drying of the surface even after the watertable started to rise again on the mid-beach. Davidson-Arnott *et al.*, (2007) notes that drying of the mid-beach occurs during the day caused by evaporation due to winds and solar radiation.

Variability on the foreshore (10-25%) occurred following a semi-diurnal pattern due to the tides, but also shorter-term variations (due wave run-up, groupiness and wave setup) (Davidson-Arnott *et al.,* 2007; Bauer *et al.,* 2009; Namikas *et al.,* 2010)

Atherton *et al.,* (2001) investigated both surface moisture and watertable variations in the cross-shore at 4 measurement stations over the period of one day and related results to thickness of the capillary fringe and specific yield. Results at the most landward located station of this study showed that surface moisture declined with a falling groundwater table. Once the water table reached a depth of about 30cm a more rapid decline in surface moisture content was observed. The more seaward located stations showed no change in moisture content, as water table remained close to the surface < 15 cm depth. While monitored during drying conditions (falling groundwater table) surface remains saturated (or close to saturated at the most landward located station) and thus groundwater table is a poor substitute of surface dryness. Hence, estimates of capillary thickness should be included. This study was carried out in a relatively fine-grained beach (150-180 μm) where the capillary fringe becomes relatively more important compared to coarser grained beaches.

Yang and Davidson-Arnott (2005) conducted moisture measurements on a beach using the Delta-T Theta probe within two grids of different size. Firstly, a large 50m by 25m grid with 50 points was established to identify along and cross-shore variability and secondly, a 1 × 1m grid with 25 points was established to identify small scale moisture variations. Results of the small-scale grid show that on the upper-beach during dry conditions moisture is uniformly distributed. However, after rainfall or tidal inundation the distribution within one square meter shows variation up to maximum 4% due to sediment packing and topographic irregularities (Yang and Davidson-Arnott, 2005).

Measurements of the large grid reveal just as results of Bauer et al., (2009) and Namikas *et al.,* (2010) largest variability in the moisture content at the fore-shore related to wave run-up and tidal inundation. Furthermore, results of Yang and Davidson-Arnott (2005) show that drying of the beach tends to be greatest in areas where moisture content was relatively high and on areas of the beach where the watertable was more than 0.5 meter below the surface.

Smit *et al.,* (2018) briefly describes some spatial and temporal changes of surface moisture content over the Egmond aan Zee beach during falling tide measured with a terrestrial laser-scanner. A cross-shore gradient in surface moisture content was observed, with varying moisture contents near the low-water line associated with the presence of a bar- trough system. Drying of the bars is much more pronounced but also drying of troughs is present. The influence of morphology on local soil moisture conditions is also highlighted by several other authors (Yang and Davidson-Arnott 2005; Oblinger and Anthony 2006; Davidson-Arnott et al., 2007; Bauer *et al.,* 2009; Namikas *et al.,* 2010;). In these studies, the moisture content mimics the topography in the sense that higher areas tend to dry more pronounced than lower areas.

Results of Oblinger and Anthony (2006) have shown that during neap tide the overall moisture content of the macro-tidal upper beach decreases, but tidal range and topography seem to have little effect on the lower beach that are characterised by near-saturated conditions. Authors accentuate in light of aeolian processes the segmentation of the fetch due to wet conditions in the troughs that act as sediment depocentres.

The overarching image with respect to the spatial and temporal variation of surface moisture content on beaches that emerges from the literature is a distribution best described by three zones, with a cross-shore gradient including dry conditions near the dune-toe and saturated conditions at the edges of the swash zone. The three zones describe the moisture distribution as follows: 1) A dry zone, always near the dune that may become slightly wetter due to accumulation of litter and plants but also rainfall and exceptionally high groundwater levels. This zone shifts (becomes larger in area) seaward during neap tide associated with a drop in the groundwater table. 2) The extend of the intermediate zone is strongly controlled by the elevation of the groundwater table and capillary flow that is subsequently controlled by tide, wave run-up and surge conditions. The topography of the beach alters moisture conditions in the intermediate zone characterised by wetter conditions in topographic low areas. 3) The saturated zone extends from the shoreline up to the edges of maximum wave run-up super imposed on the tidal inundation.

2.7 Entrainment Thresholds, Transport and Surface Moisture Content

An increasing number of studies highlights the complexity of sediment entrainment processes by wind, especially when surface moisture constitutes a potential control on the entrainment threshold of motion (McKenna-Neuman and Nickling, 1988; Davidson-Arnott *et al.,* 2007; Davidson-Arnott and Bauer, 2009). In this section processes related to a moisture dependent threshold are described as well as in the last part some physical relations are given as described by Delgado-Fernandez (2011) and Ellis and Sherman (2013).

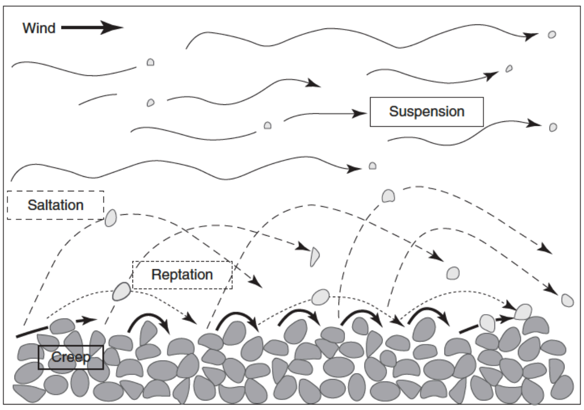

Figure 2.6 Modes of Aeolian transport, adapted from Sherman and Ellis (2013).

Entrainment of individual grains happens when forces of the wind exceed forces on those grains that resist the motion. Usually, with an increasing air flow over a sediment surface, more exposed or smaller grains are first entrained by drag (or shear stress) of the moving air. The moment of first movement of the sediment is defined as the static threshold of transport (Ellis and Sherman, 2013). This first movement of particles happens either as surface creep (rolling) or saltation (bouncing), or reptation which is somewhat ambiguously described as a transport mode between creep and low-energy saltation (Figure 2.6) (McKenna-Neuman and Nickling, 1988; Ellis and Sherman, 2013). When wind flow further continues, other grains (including larger grains in the distribution) are moved either by the imposed air flow, or by impact of earlier entrained grains (McKenna-Neuman and Nickling, 1988, Delgado-Fernandez, 2010). On moment of impact, the shear velocity threshold necessary for entrainment is reduced (dynamic threshold), since momentum of the impacting grains is transferred to grains on the surface. As a consequence, there is a cascade or avalanche effect of initially entrained particles (with varying grainsize) setting in motion a rapidly increasing number of grains resulting in rapidly increasing transport values with distance from the upwind boundary where the first grains are entrained. This continues until eventually fully developed or equilibrium transport is reached at some distance downwind from where the first particles were entrained, under these circumstances grain entrainment is dominated by impact of other grains rather than by wind shear (McKenna-Neuman and Nickling, 1988; Bauer *et a.l,* 2009; Delgado-Fernandez, 2010). The particle flux modifies the wind flow near the bed, creating an internal boundary layer that grows downwind. As a result, when the critical fetch length is exceeded this self-balancing mechanism limits the further growth of the saltation cloud and equilibrium transport is reached (Delgado-Fernandez, 2010).

It was found that a single value for shear velocity threshold does not properly reflect observations on natural beaches, even without considering spatial and temporal variability in moisture or other complicating factors (McKenna-Neuman and Nickling, 1988). The threshold of shear velocity is in natural sediments best defined by a range of values reflecting the grain size distribution and considering either a static or dynamic threshold for a minimum wind speed (McKenna-Neuman and Nickling, 1988). McKenna -Neumann and Nickling (1989) indicated that when surface moisture is considered as a potential control, the soil water characteristic curves of sand samples hold close resemblance to the variation in threshold shear velocity with moisture content.

Next to many other factors that affect the threshold for sediment mobilization (e.g: microbiotic (Arens, 1996; McKenna-Neuman and Langston 2006) and/or salt crusting (Nickling and Ecclestone, 1981; McKenna-Neuman and Langston 2006), sediment packing, grain-size, shape and sorting (Rice, 1991), salt concentration (Nickling and Ecclestone, 1981), vegetation (Wolfe and Nickling, 1993) and presence of shells and natural or antropogenic debris and presence of snow and ice Delgado-Fernandez (2011)) surface moisture is widely acknowledged as an important control in increasing the shear velocity threshold needed to mobilize sediment on beaches (Nickling and Ecclestone, 1981; Davidson-Arnott *et al.,* 2008; Bauer et al., 2009; Nield et al., 2010).

This observation is confirmed by many wind tunnel experiments that reveal a steep increase in shear velocity with moisture content (Cornelis and Gabriels, 2003). However, the relatively simple and static moisture conditions adopted in most wind tunnels studies fail to account for the dynamic behaviour of the threshold on natural beaches (Davidson-Arnott *et al.,* 2007; Wiggs *et al.,* 2004). The high degree in spatial and temporal variation of moisture content together with unsteady wind conditions on natural beaches make it difficult to model a threshold condition that determines the area potentially available for aeolian transport (McKenna-Neuman and Langston 2006).

Many aeolian transport models that predict the transport rate (q_s) include empirical constants and perform predictions for ‘ideal’ conditions including non-cohesive sediments of uniform size and density with horizontal unobstructed surfaces (Bagnold, 1941; Lettau and Lettau, 1977). Despite the physical justification of the models, many over-predict transport rates even when some of the models include a threshold velocity component (Ellis and Sherman, 2013). Large parts of the errors in these kinds of models emerge due to the assumed transport (rather than supply) dominated saltation that is in equilibrium with the wind field (Ellis and Sherman, 2013). Later, some models including supply-limited transport systems were developed, where homogenously distributed moisture restrains the development of equilibrium transport (Nickling and Ecclestone, 1981).

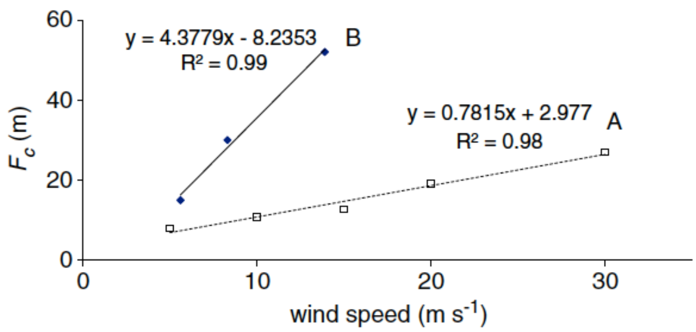

Figure 2.6 Correlation between the critical fetch distance and imposed wind speed based on data of A) Davidson-Arnott and Law (1996) and B) Spies and McEwan (2000).

On wet beaches equilibrium transport may never be attained, since the fluid stresses (and some other factors) decrease the number of grains ejected by the wind, resulting in a smaller number of grains in the saltation cloud that subsequently decreases the number of grains dislodged by other previously entrained particles, making for a slower increase in transport rate down wind on a moist beach compared to a dry beach (Delgado-Fernandez, 2010). Observations on wind speed and critical fetch length of Davidson-Arnott and Law (1996) suggest that during high wind speeds over wet beaches the critical fetch becomes larger following a linear trend as depicted in Figure 2.6. Under these high wind speed circumstances the critical fetch distance is usually greater than available fetch, which is limited by the width of the beach. However, as argued by de Vries *et al.,* (2014) supply limiting factors, especially moisture could dominate over the fetch effect especially because supply rates and wind speed can vary both on very short time-scales which makes the determination of a critical fetch distance difficult. This, however contributes to the current understanding of the importance of surface moisture variability as supply limiting factor.

A number of studies have tried to conceptualise and model the working mechanisms of a moisture dependent threshold (Davidson-Arnott *et al.,* 2009; Wiggs *et al.,* 2009; Delgado-Fernandez, 2011) of which Belly (1964) is one of the most frequently deployed of modelling studies (Ellis and Sherman, 2013). During relatively low moisture conditions the most important threshold parameter on saltation activity is wind speed and the system is transport limited (Wiggs *et al,* 2004, de Vries *et al.,* 2014). However, when surface conditions are damper a more dynamic threshold parameter best describes saltation activity and the system becomes supply limited (Cornelis and Gabriels, 2003; Wiggs *et al.,* 2004). Davidson-Arnott and Bauer (2009) note that once transport becomes well established, the sensitivity of entrainment to differences in moisture conditions between 1-2% is small and entrainment is dominated by grain impacts and wind speed.

Wiggs *et al.* (2004) showed that surface moisture was the dominant control on saltation activity for over an hour, but when surface conditions dried to a certain extend the wind velocity resumed control in determining whether saltation occurred or not. Therefore, the shift rapidity of dominant controlling factor strongly depends on drying rate of the surface which is in turn determined by environmental factors that make for a shift in threshold condition over a period from minutes to hours (Wiggs *et al.*, 2004; Davidson-Arnott *et al.*, 2008).

These results are in line with previous findings of Jackson and Nordstrom (1997) who to noted that the drying process associated with rapid evaporation obscures the relation between transport rates and surface moisture content. It is also suggested that the drying process of the very surface might be a more important control on the entrainment than moisture content itself (Sherman, 1990). However, sand entrained (depending on the moisture content and windspeed) after being exposed to some degree of evaporation requires next to the evaporation rates information on initial moisture conditions if evaporation rates would hypothetically be considered. Another obscuring factor emerges due to aeolian deposited bedforms, which usually consist of very dry sediment (sediment dries considerably when being transported) but the source might be from a moist surface, which next to rapid surface drying results in large moisture gradients over a small depth (Jackson and Nordstorm, 1997).

During conditions of damp sediment and turbulent wind close to the threshold of motion intermittency of saltation activity becomes apparent (de Winter *et al.,* 2018; Davidson-Arnott *et al.*, 2008)). However, intermittent transport could also be explained by short term moisture fluctuations in the uppermost surface layer even under steady wind conditions (Bauer and Davidson-Arnott, 2009). The uppermost surface layer of sediment rapidly (in minutes) dries after which it is more easily removed. Revealed is a 'new' surface with wetter sediments that will start to dry and eventually are removed again. This phenomenon will repeat itself causing and intermittent signal in transport activity (Cornelis and Gabriels, 2003).

These short-term moisture gradients in the very uppermost sediment layer might be hard to recognize using conventional depth-integrated moisture measurement techniques (Nield *et al.,* 2011; Edwards *et al.,* 2012). In addition, these measurements techniques cannot characterise the moisture distribution over a continuous horizontal plane (Smit *et al.,* 2018*)*. Careful observations of this process include instantaneous and continuous measurements of surface moisture and surface height. The usage of a terrestrial laser-scanner as used by Smit *et al.* (2018) may hold promising advantages in future studies that focus on beach moisture variability and define moisture dependent entrainment thresholds.

Despite the complexity and many interrelated processes that constitute a control on the entrainment of sand particles, some authors proposed expressions in which the surface moisture content alters the entrainment threshold and ultimately aeolian transport q_n in (m^3s^{-1}). In a study of Delgado-Fernandez (2011) that assesses different modelling steps a classification of moisture content before critical fetch F_c and transport q_n calculations are performed is proposed. In this model 0 - 4% is classified as dry where no alteration of the critical fetch is performed because rapid surface drying and subsequent sand stripping were assumed under these conditions (Cornelis and Gabriels, 2003; Delgado-Fernandez, 2011). In this model both equilibrium and disequilibrium transport calculations are altered by the moisture content, via incorporating the theoretical fetch effect.

Equation 2.5 shows the dependence of wind speed on the critical fetch as visualized based on observations of Davidson-Arnott and Law (1996) in Figure 2.6.

$$F_c = 4.38 \times U - 8.23 \qquad (2.5)$$

In which U is the wind speed in (m/s). The critical fetch distance is here defined as the distance from first particle entrainment (required for the saltation cloud to develop) to the point (or line) in space where fully developed equilibrium transport is encountered. Under dry conditions (0 - 4%) this distance linearly increases with increasing wind speeds and stronger winds require a wider beach before equilibrium transport may occur Davidson-Arnott and Law (1996).

Based on a model developed for meso-scale modelling purposes the critical fetch distance during moisture conditions of 4 - 6 % is increased by 0.5 of the original, dry sand fetch distance which is dependent on wind speed alone as described in Equation 2.5. adapted from (Delgado-Fernandez, 2011). During moisture conditions ranging from (6 - 10%) the critical fetch distance is increased with 0.75 of the original fetch. With moisture conditions above 10% it is assumed that no transport occurs for any wind speed.

Subsequent transport calculations are performed after the critical fetch is compared to the available fetch. When $F_c \leq F$ wind speed and direction are used to calculate potential transport per unit alongshore distance (Equation 2.5). If $F_c \geq F$ equation 2.6 is employed. Hourly data is subsequently summed to calculate total transport Q (Delgada-Fernandez, 2011).

$$q_n = 1.16 \times 10^{-5} \times U^3 \cos(\alpha) \quad (2.5)$$

$$q_n(F) = q_n \sin\left(\frac{\pi}{2}\frac{F}{F_c}\right) \quad (2.6)$$

In the previously discussed models, the wind velocity rather than shear velocity is used to calculate potential transport. Including the shear velocity requires knowledge on the roughness length (z_0) that varies spatially and temporally (Davidson-Arnott and Law, 1996). The following formulation of an entrainment threshold is based on shear velocity calculated from the Wall of the Law following Ellis and Sherman (2013).

Initiation of motion is generally defined as the circumstance when the shear velocity (u_*) exceeds the threshold shear velocity (u_{*t}) where the threshold shear velocity is largely dependent on mean grain diameter (*d*) and the square root of the Shield's parameter following Bagnold (1936).

$$u_{*t} = A\sqrt{\frac{\rho_s-\rho}{\rho}(gd)} \quad (2.7)$$

In equations 2.7 Where ρ_s is grain density for spherical grains of uniform size, ρ the density of the air and *g* gravitational acceleration. As described above, the value of A corrects for the energy required to initiate movement of a grain when no other particles are saltating (static threshold) or when other particles are saltating (dynamic threshold). For a static threshold A is set to 0.1 and for a dynamic threshold 0.0082 is assumed (Ellis and Sherman, 2013).

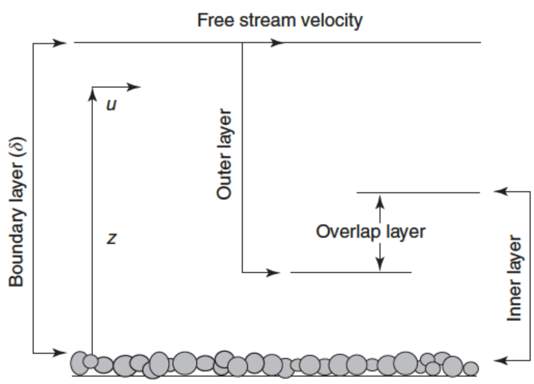

Figure 2.7 The atmospheric boundary layer, vertical logarithmic wind speed decrease as described by the Law of the Wall (Adapted from Ellis and Sherman, 2013). (image is not to scale)

To evaluate if the threshold shear velocity is exceeded, the shear velocity due to a certain wind speed is derived. The von Kármán logarithmic velocity profile equation that describes the inner layer of the atmospheric boundary layer is typically used in studies to the initiation of sand motion by wind (Figure 2.7). Aeolian studies concerning wind speed fluctuations mainly focussed on quantifying the change of wind speed with distance from the bed, typically used the boundary layer theory or 'Law of the Wall' by Prandtl and von Kárman (Ellis and Sherman, 2013). The theory quantifies a logarithmic relation between wind speed and height above the bed (Equation 2.8), the vertical region from the bed surface to the height where the wind speed reaches 99% of the free stream velocity is defined as the boundary layer (Ellis and Sherman, 2013).

$$\frac{u_z}{u_*} = \frac{1}{k} ln \frac{z}{z_0} \qquad (2.8)$$

where u_z is wind velocity *u* at height *z* (0.9m in this study), *k* is von Kármán's constant typically 0.42 and z_0 is roughness length (estimated as 1/30th of the mean grain diameter which is assumed the height above the bed where the wind velocity equals zero) (Ellis and Sherman, 2013).

In order to correct for the effects of moisture on the threshold shear velocity the following equation (2.9) proposed by Belly (1964) based on an empirical fitting procedure is commonly used in combination with equation 2.7 and 2.8 (Namikas and Sherman, 1995). With w gravimetric moisture content (%). Here u_{*tw} is the threshold shear velocity based on grain density, grain size and corrected for present moisture that hampers the entrainment.

$$u_{*tw} = u_{*t}(1.8 + 0.61 log_{10} w) \qquad (2.9)$$

Some authors note that the use of this equation is only applicable in the range of moisture content between 7% and 14% (Ellis and Sherman, 2013). Sarre (1984) noted that moisture levels less than 14% in the top few millimeters of the sediment were seen to have little effect on the transport. It should be noted that this author used a different moisture correction factor that was incorporated into flow intensity equations based on wind shear (Kadib, 1965).

Transport equations that can subsequently be used (and were previously used by some other authors Ellis and Sherman, 2013; de Vries *et al.*, 2014) that describes aeolian transport altered by moisture and shear velocity, as described by the following expression (Equation 2.10) proposed by Lettau and Lettau (1978).

$$q = \alpha C_b \left(\frac{d}{D}\right)^{0.5} \frac{\rho}{g} (u_* - u_{*tw})^3 \qquad (2.10)$$

With q transport rate in (kg/s/m (width)), D reference grainsize (mm), d grain diameter (mm), ρ air density (kg/m^3), g gravitational acceleration (m/s^2) and C_b = typically set 1 - 2 in wind tunnels and depending on sorting of the considered sand (Lettau and Lettau, 1978; de Vries *et al.*, 2014). It should be noted that this (equation 2.10) is normally used in steady wind conditions when sediment supply is ample. However, with considering surface moisture that alters the dry threshold shear u_* to wet threshold shear $u_{*\,tw}$ as proposed by belly (1964) (equation 2.9) a supply limiting factor is incorporated in the model. However, spatial and temporal variation of this supply limiting factor is not included (homogenous moisture in space and time are assumed under steady wind flow conditions).

In summary from literature became apparent that entrainment of sand by wind is a complex process that is altered by surface moisture content and not yet fully understood. Surface moisture content as measured integrated over 2 cm depth can be a surrogate for the actual top few millimeters of sand but should be used with caution since large gradients in moisture that fluctuate over short time-scales might be present. Nevertheless, entrainment thresholds as proposed in literature were found to lie at 10 and 14% moisture.

2.8 Main Objectives

From the literature presented previous section became apparent that marine, atmospheric and subsurface processes influence the surface moisture distribution of the beach. The distribution can be divided in three different zones. A wet zone, characterized by saturated conditions. This zone shifts across the beach depending on the tidal level and wave run-up. The second zone of intermediate wetness arises due to subsurface and atmospheric influences, where the balance between gravitational drainage, capillary flow and atmospheric conditions mostly determine the surface wetness. In contrast to the first zone, the groundwater table is situated below the surface, deeper than the thickness of the capillary fringe. However, in the intermediate zone some capillary water reaches the surface. In the third, dry zone moisture conditions are characterized by the field capacity of the sediment where only very small amounts of capillary water remain in the sediment.

Furthermore, from literature became apparent that the depth of the groundwater table is important for surface wetness as described by the soil water characteristic curve. However, on beaches it is not only the groundwater table depth that varies, but also the surface level of the beach is non-static due to morphodynamic interactions between the bed and water currents. These interactions control surface elevation of the beach which subsequently alter the beach wetness by modulating the depth of the groundwater table below the surface. Therefore, it is not only variation in the groundwater table elevation (and capillary thickness) but also the morphological variation of the intertidal beach that should be considered when studying the spatial and temporal variation of surface moisture on a beach.

Variations in the surface moisture distribution pose a potential control on the entrainment threshold and development of equilibrium transport via the fetch effect because water in the sediment pores increases the interparticle cohesion. Typically, present surface moisture content was classified and used to modify equations that calculate either the critical fetch distance or the wet threshold shear velocity. In meso-scale studies these modifications are used to ultimately alter predicted sediment rates. However, no other studies focussed on incorporating a parameter that predicts the potential area available for aeolian transport for a certain wind speed due to spatio-temporal shifting of the threshold zones that alter the critical fetch distance or pick-up rate of the sediment and subsequent transport.

Especially variability of the intermediate zone, where conditions are neither saturated or dry around the threshold of entrainment for different wind speeds, are important to understand. In addition to drying associated with gravitational drainage, solar radiation and other environmental factors a complex relationship between wind gusts, drying and stripping of surface grains exists which alters the threshold condition on a temporal scale from seconds to minutes. Furthermore, the entrainment threshold is altered by impact of other saltating grains, which complicates determination of aeolian entrainment conditions and determining a critical fetch distance on natural beaches.

Only a few studies described and quantified surface moisture variation as it changes in time and space across a beach. It is due to the large number of processes and interactions between these processes that only relatively little is known about the variation. This lack of knowledge is thought to contribute to the current inability to accurately predict long-term (months to years) sediment fluxes from beach to fore-dune and hamper the ability to close the coastal sediment budget which is an important aspect for decision and policy makers in coastal management positions.

The objective of this study is to observe, quantify and describe in terms of governing physical processes the spatial and temporal variation in surface moisture content. Firstly, variation on a time-scale from hours to weeks is assessed by allocating important environmental processes (and 'sub-processes') that cause the variation. Processes that are extensively studied include the effect of the tidal level, the beach morphology and the effect of storm surges. Where after, the effect of surface moisture content on the entrainment threshold is studied. In this manner, this study aims to determine how surface moisture could be considered in future attempts to model aeolian processes. Bearing these aims in mind, the following research questions are synthesized.

1. How does the surface moisture content of an intertidal beach vary in space and time?

- A) How does the tidal cycle influence the surface moisture content?
- B) How does the evolution of the intertidal beach morphology influence the surface moisture content?
- C) How does the spatial and temporal variation in drying of the beach after a storm surge take place?

2. How does surface moisture influence the entrainment threshold of sand for aeolian transport?

- A) Is there a critical moisture content where above no entrainment takes place and where below aeolian activity starts?

3. Methodology

3.1 Aeolex II

This MSc-research was conducted in the framework of Aeolex II, a field study on aeolian processes operated by the Physical Geography Department of University Utrecht. The overarching aim of this project is to investigate how properties of the wind, beach and sand control the timing and quantities of aeolian sediment transport, which ultimately determine the natural recovery of the dunes after severe storms. The field campaign was executed from October 1 to November 3, 2017. Field measurements on various variables that control the beach-dune sediment budget were conducted by four MSc students under supervision of staff members of the Physical Geography Department. Topics of the four studies include 1) The effect of vegetation on changes in aeolian transport and wind characteristics over the fore-dune. 2) Variability in wind speed and direction over the intertidal beach. 3) Saltation intensity and aeolian mass flux variation over the beach. 4) Spatial and temporal surface moisture variability across an intertidal beach.

Variables that were measured for the broader research project include: tidal water level, groundwater table elevation, ambient air temperature, in- and outgoing solar radiation, relative humidity, air pressure and rainfall. Furthermore, 3-dimensional wind speed and direction were measured using three mobile sonic anemometers and three static sonic anemometers (static anemometers were located in a transect at the foredune and the mobile anemometers were positioned depending on prevailing environmental conditions). Furthermore, two cup anemometer masts that measured wind direction and wind speed (at several vertical logarithmically distributed heights) were installed at the intertidal beach and in front of the fore dune. Furthermore, periodic observations of surface moisture content, morphology, saltation intensity, aeolian mass flux and vegetation cover were obtained.

Figure 3.1 Top left, staff members and students loading the instrument container at the start of the campaign. Top right, saltation detection system with ultrasonic anemometer and right of the set-up are faintly visible two moisture markers. Bottom left, field site with groundwater wells, static and mobile ultrasonic anemometers and the meteo-mast (right side of the picture). Bottom right, capturing the beach profile (morphology) with a mobile RTK-GPS along the well transect (note soil moisture marker next to student).

3.2 Field Site

The field site was located some 3 km south of Egmond aan Zee (Figure 3-2) on the approximately 120km long and almost uninterrupted Holland coast. On this large scale, the wave-dominated beach can be characterised as alongshore uniform and compromises three subtidal sandbars (Pape *et al.,* 2010). The coast at Egmond aan Zee is approximately North-South orientated (8.32 degrees clockwise rotated) and predominantly exposed to North-sea generated wind-waves (De Winter *et al.,* 2015). The climate in the Netherlands is temperate humid with strong seasonal influences. Stormy season occurs in the months October to February, with wind directions predominantly from the West, Southwest and Northwest. During these directions, mild and wet conditions usually occur alternated with often colder periods and moderate winds from the East (Arens, 1996).

At the study-site a fairly flat beach profile (1:30, see Figure 3.3B) bordered by a continuous fore-dune of about 18 m in height is present. Vegetation cover consists of mostly in Marram grass (*Ammophila Arenaria*) and sand couch-grass (*Elymus Factus*). Tides are semi-diurnal and the range is about 1.5m but water levels vary with spring-neap cycles and wind and wave conditions, holding that large part of the beach is flooded twice a day. During storm surges, that most significantly happen during north-westerly storms the beach may be flooded all the way up to the fore-dune, during these conditions the foredune is prone to erosion (Figure 3.6).

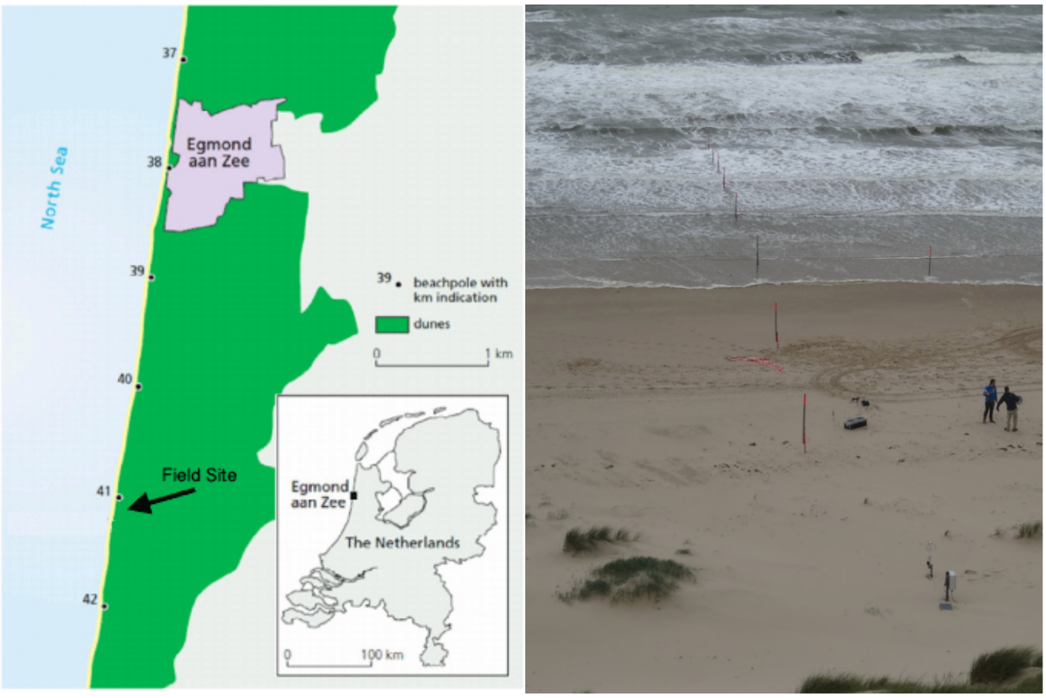

Figure 3-2 On the left, maps indicating the location of the field site in the Netherlands, adapted from Smit et al. (2018). On the right, a picture taken from the crest of the fore-dune. Note the groundwater wells (middle) with a mobile sonic anemometer next to the most landward located well and the first stationary sonic anemometer at the dune-toe (lower right corner). Photo courtesy of prof. dr. Gerben Ruessink.

Sieving results from the field site collected sand samples and subsequent textural analysis using GRADISTAT (displayed in Figure 3-3A) show that the Egmond aan Zee sand is well to very well sorted, medium to fine sand (225 to 304 µm). Some cross-shore spatial variability is present as reflected by the most seaward located sample, that is slightly less well sorted and coarser as reflected by the higher D_{90} were both D_{10}, D_{50} and D_{mean} follow the same landward cross-shore decreasing trend.

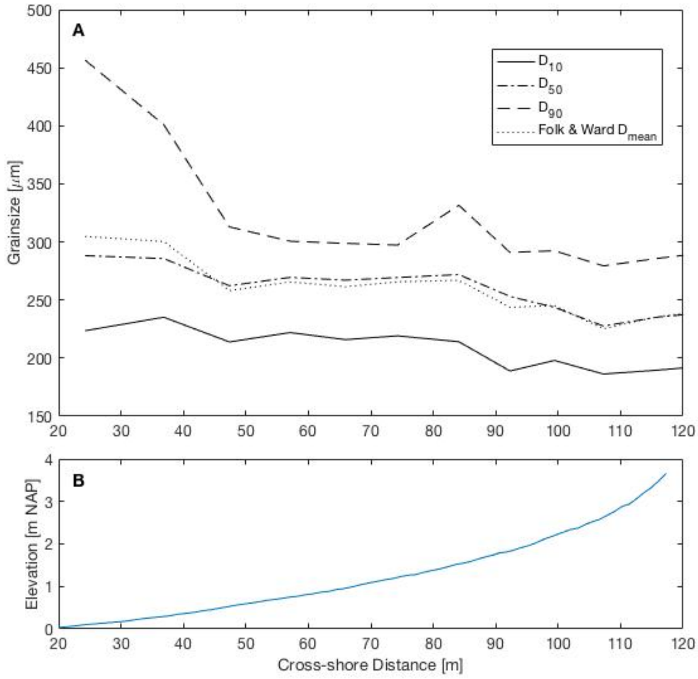

Figure 3-3 A) Cross-shore distribution of D_{10}, D_{50} and D_{90} grainsizes, and B) the beach- profile as measured on October 31, the day the grainsize samples were collected.

3.3 Boundary Conditions

During the field period, atmospheric variables that might influence the surface moisture conditions are measured at the field site using the meteorological-mast, depicted in the bottom left picture of Figure 3.1. An overview of the meteo-data collected during the field-period is given in Figure 3.4. Panel A shows the temperature changes over the course of the field period, note the warm day during October 16. These exceptionally warm temperatures are associated with storm Ophelia that hit Ireland during this period also made for calm conditions on the North-sea. Panel B shows the diurnal cycles of the incoming solar radiation and C displays the amount of precipitation as measured with a tipping bucket from the October 12 onwards.

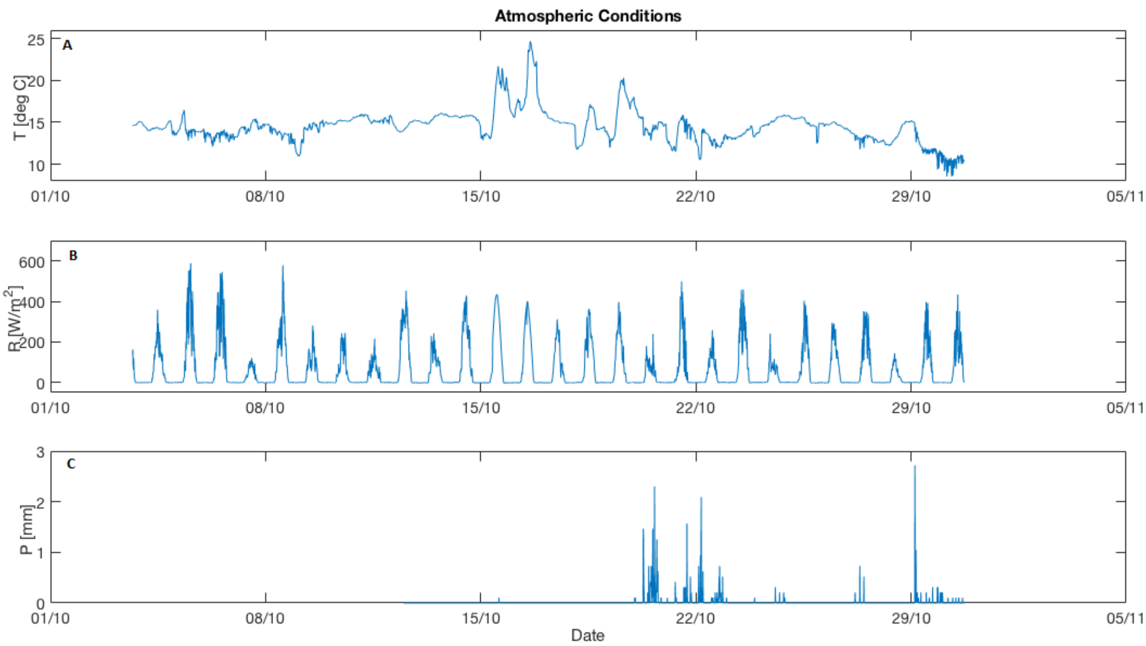

Figure 3-4 Atmospheric conditions as measured from the meteorological-station on the field site. A) Temperature in °Celsius B) The incoming solar shortwave radiation in W m^{-2} and C) Precipitation in mm.

During the field-campaign off-shore oceanographic boundary conditions were obtained from the IJgeul stroommeetpaal operated by the governmental institution Rijkswaterstaat. The location of the measurement station is about 2.5 km offshore near IJmuiden, which is some 15km south of the study site. The variables from this measurement station are shown in Figure 3-5. The wave angle of incidence is measured at another nearby station.

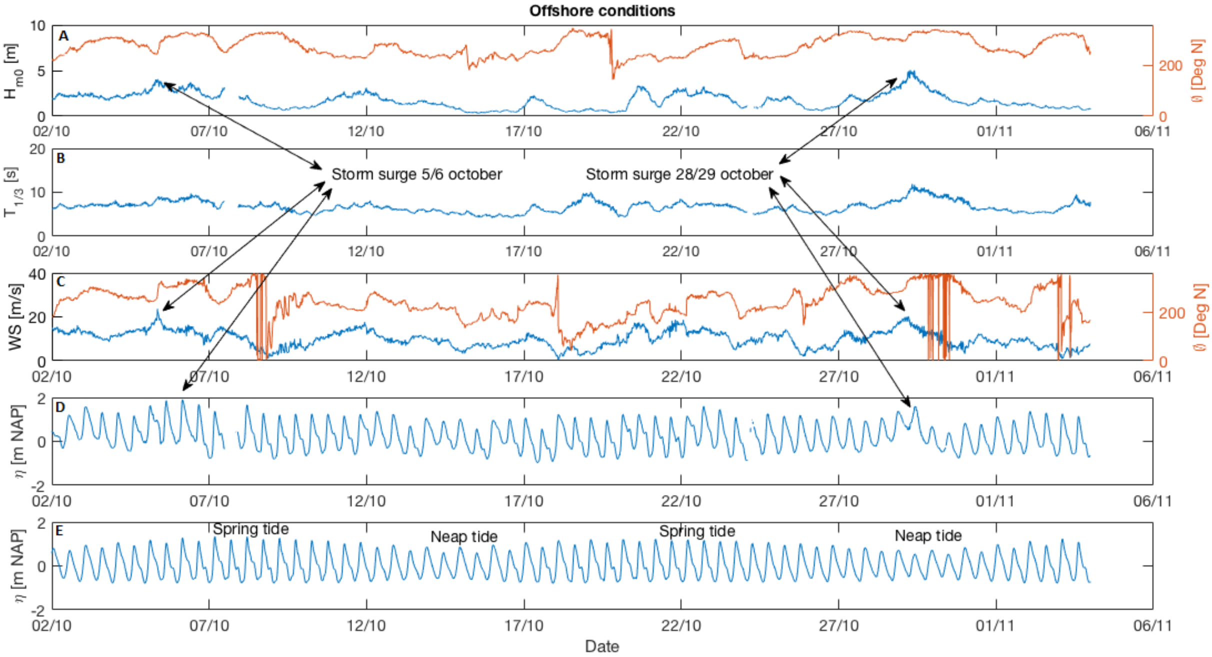

Figure 3-5 Offshore measured oceanographic boundary conditions during the field period. A) Significant wave height (m) and wave angle of incidence (Deg N). B) T 1/3 (s) wave period. C) Wind speed (m/s) and wind direction (Deg N). D) Water levels measured at open sea (m NAP). E) Astronomical tide (m NAP). Indicated are two storm surges and spring and neap timing in panel E.

Wind, wave and water level conditions are marked by two north-westerly storms at the start and at the end of the field period that both happened during the night-time of (October 5 and 28) with mean wind speeds (averaged over 10 minutes) over 20 m/s and maximum significant wave height reaching 5 m during the last storm. The water level rise due to the surge can be obtained by looking at the difference between the measured water levels (panel E) and the astronomically predicted tide (panel D) which in both cases is over 1 m. Furthermore, note the increasing wave period and height during the north-westerly storms. The left panel of the following figure (Figure 3.6) gives an impression of the dune erosion that happened after the first storm surge. In contrast to the stormy conditions, from around October 13 to 19 fair weather conditions prevailed, with low wind speeds (< 4 m/s) and small significant wave heights (< 1 m). Note how the longer period swell (10 seconds) is measured on October 18, it is during these fair-weather conditions that the intertidal sandbars tend to grow and migrate shoreward, see right panel of the following Figure 3.6.

Figure 3-6 Beach during Stormy and fair-weather Conditions. Left panel, looking south, erosion of embryo dunes during the storm-surge on October 6 (at this part of the beach, north of the study site the embryo dunes have grown exceptionally wide and extend several meters seaward from the fore-dune). Right panel, looking North, formation of intertidal sandbars at the study site after fair-weather conditions, as captured on October 16.

3.4 Data-collection and Processing

Variables important for this research and that were continuously collected during the field campaign include: sea surface elevation, groundwater table elevation, wind speed and direction, temperature, incoming solar radiation, air pressure and rainfall. Furthermore, periodic measurements of the surface moisture content, morphology and saltation intensity were conducted. For an overview of each measurement station and their measured variables, operating period(s), sensor types and locations the reader is referred to Appendix. The remaining of this section discusses the operation principles of the data-collection devices, the field methods and the steps taken to process the data to usable output.

3.4.1 Surface Moisture Content

In order to tackle the research questions surface moisture content of the beach was measured using three different sampling locations. Firstly, to study the surface moisture variation in relation to tidal inundation and subsequent groundwater level variation, the moisture measurements were conducted along a cross-shore installed groundwater well transect (as depicted in Figure 3.2). Secondly, to study the entrainment threshold in relation to the surface moisture content, measurements were conducted in front of and perpendicular to a saltation detection system (SalDecs). Thirdly, to relate the surface moisture conditions and intertidal beach morphology a sampling grid that captured the edges of a trough and associated intertidal sandbar were sampled. Each of the sample locations and sample methods are further elaborated upon later in this section. Firstly, the working mechanisms, calibration and accuracy of the measuring device that was used to measure the surface moisture content throughout the field period is outlined.

Modification of the Delta-T Theta Probe

All three sampling methods were performed using the same Delta-T theta probe (type HH2). The device consists of a read-out unit in a waterproof housing that contains the electronics, which is connected to the sensor via an electric cable. The sensor has 4 stainless steel rods of 2cm long that are inserted into the sediment. The rod length is originally 6 cm but shortened to measure only the uppermost moisture content important for this study. 2 cm is chosen as a compromise between measuring as close as possible to the surface and decreasing precision with further rod length reduction. The reduction in rod length is similar to modifications adapted by other authors who used di-electric foam (Tsegaye *et al.,* 2004; Davidson-Arnott *et al.,* 2008; Namikas *et al.,* 2010; Schmutz and Namikas, 2011). For more information on operation principles of the probe, the reader is referred back to chapter 2.6 or the user manual of the Delta-T theta probe type HH2 (Delta-T Devices, 2005).

Calibration of the probe

The output of the probe ranges between 0 mV and 800 mV (dry and fully saturated). To relate the probe's output to moisture content, a calibration was performed. Beach sediment samples at arbitrary locations on the beach were analysed with the probe until the entire output range was captured. At each measuring location, the sample was collected with a shallow coring ring with same diameter and depth as the probe's rods. The samples were bagged and immediately sealed for transport. Protocols of standard gravimetric moisture analysis were followed; the wet mass of each sample was determined after which the samples were dried in the oven for 24hrs at 105 °C. After drying, the mass of the samples was determined again. The fraction of wet mass over dry mass times 100% is defined as the gravimetric moisture content of the sample. This procedure was followed at the start and end of the of study period for the same probe that was used for all moisture measurements.

Results of the two calibrations are shown as ensemble in the following figure (Figure 3-7). A fourth order polynomial regression is used to describe the relationship between moisture content and probe output. With a R^2 value ≈ 0.98 the equation of this curve is used to transform output results to gravimetric moisture content throughout this thesis. The standard error of the probe as calculated from $SE = \frac{\sigma}{\sqrt{n}}$ with σ the standard deviation and n the number of observations, and reveals 1.17%. Apparent from the curve becomes that the device is most sensitive to moisture conditions in the range of 0 to 18% moisture, beach conditions with more than 18% moisture indicate increasing levels of (over)saturation. In cases of oversaturation the volume of water in the pores exceeds the volume available in the pores of the sediment. From visual appearance in the field it is expected that sediments become fully saturated around 18% moisture.

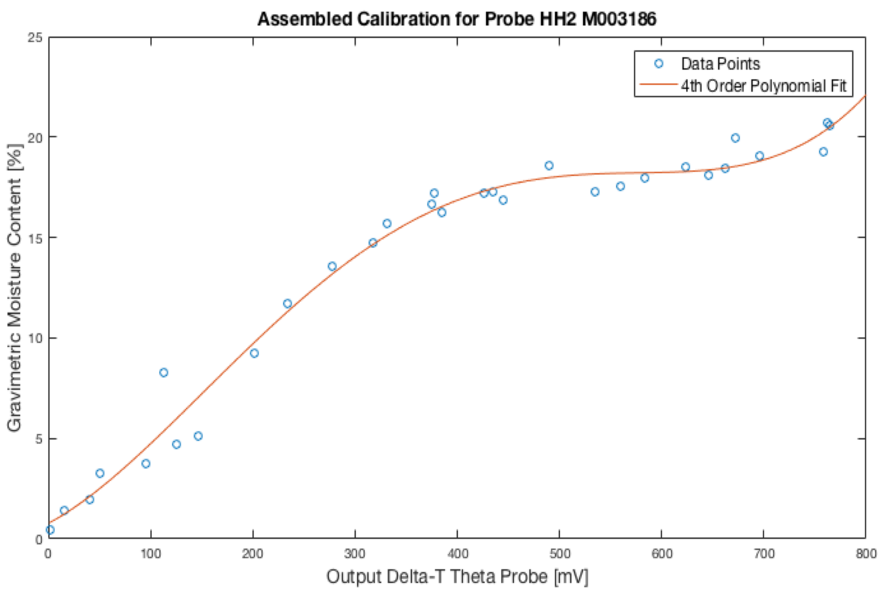

Figure 3-7 Calibration curve of Delta-T Theta probe, a fourth order polynomial describes the sample points with a R-square value ≈ 0.98 and RMSE ≈ 0.92 and SE = 1.17%.

Accuracy of the probe

At each measurement location, which was an area of about 15 by 15 cm around a marker, five probe measurements were conducted and averaged to correct for small scale variations and instrument noise, this was done in all following sampling methods 1, 2 and 3. Comparing the standard deviation with the mean moisture content of these 5 measurements (Figure 3-8), variability due to small scale variations or instrument noise is investigated. The figure reveals for low moisture contents a relatively small standard deviation, mostly below 0.5%. Moving toward intermediate wetness more scatter and more small-scale variability due to instrument noise is present. For wet conditions the standard deviation reaches below 0.5% again. This distribution of the standard deviation resembles a normal distribution, as was found by other authors (Edwards and Namikas, 2009).

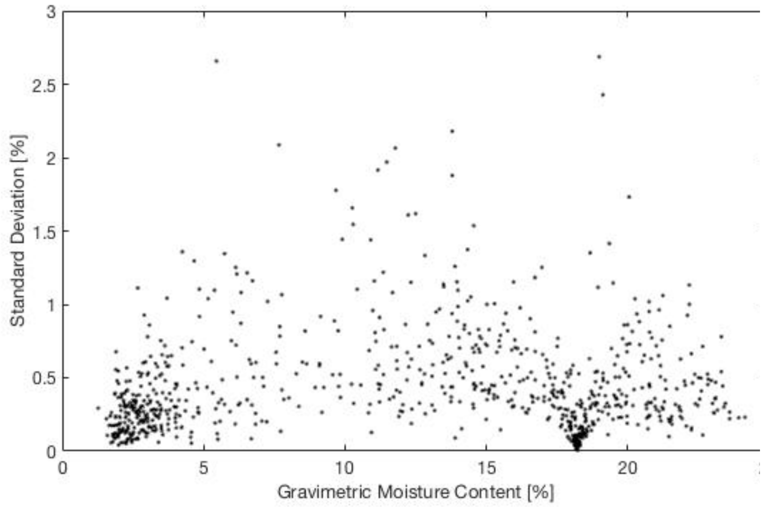

Figure 3-8 Standard deviation of the five measurements plotted against mean moisture content of the five measurements.

Clustering of the data around 18% moisture is due to the small slope in the calibration curve (Figure 3-7). This moisture level corresponds to a rather large output range of the probe (approximately from 600 to 800 mV), making for the small standard deviation at this moisture level. When sorting the standard deviation data using a spreadsheet, it becomes apparent that 94% of the data has a standard deviation smaller than 1% moisture and 76% of the data has a standard deviation smaller than 0.5% moisture indicating that in general the small-scale variation or reader noise is small (mostly <0.5%) compared to the beach-scale variation (0 – 25%).

Sampling method 1

Surface moisture measurements along the cross-shore transect of groundwater wells (Figure 3-9) were performed in order to study the forcing nature of the tides and beach groundwater table. The moisture measurements were employed with a smaller spacing (about 5m) between each subsequent location compared to the spacing of the wells, as displayed in the following figure. The groundwater wells were also used as soil moisture markers. On these locations, the surface moisture content could be directly related to the depth of the groundwater table. Furthermore, parameterization of the proposed van Genuchten (1980) expression (Equation 2.2) was performed using a nonlinear least-squares regression that optimizes the curve on coefficients α and n, where θ_s and θ_r are fixed parameters determined from the field observations.

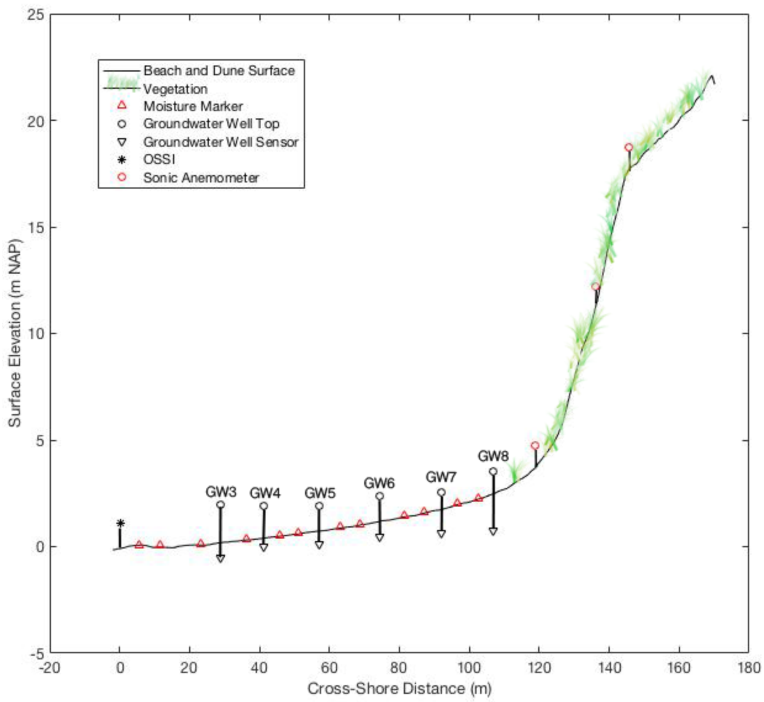

Figure 3-9 Cross-shore profile of beach and dune with instrument locations including; the "OSSI", the surface moisture markers, groundwater wells and stationary sonic anemometers on the fore-dune. The groundwater wells are displayed as the set-up after the first storm on October 6, of which the most shoreward (GW3) and the four most landward located (GW5, GW6, GW7 and GW8) continuously measured groundwater fluctuations throughout the field period.

Employing the sampling method as previously discussed with five measurements per marker, each location could be handled in about 45 seconds, holding that the entire transect consisting of a maximum of 24 markers during low tide could be handled in less than 20 minutes. Depending on the inundation level of the beach the entire transect was measured in much shorter time.

The locations of the other markers (in between the wells) are more or less consistent every measurement day, with approximately equal spacing between each location. However, the markers had to be removed with every incoming tide and replaced for the next measuring day. Therefore, the spacing and number of locations in between the groundwater wells varied slightly each measurement day. The locations (xyz) were obtained after each new transect was placed using the RTK-GPS and transformed to a local grid as described later in this chapter (section 3.3.4). Days on which moisture measurements were carried out following this method include October 6, 9, 10, 12, 16, 22, 24 and 26.

Sampling method 2

Moisture sampling method 2) was carried-out on days with aeolian activity, when saltation detection stations (SalDecs) were deployed in combination with sonic anemometers to measure saltation intensity and 3-dimensional wind speed. Moisture content was measured in front of a SalDecS by means of a transect (Figure 3.10). In addition to the principles followed in method 1, at each moisture measurement point was noted if visually any transport happened during the +-45 seconds of sampling.

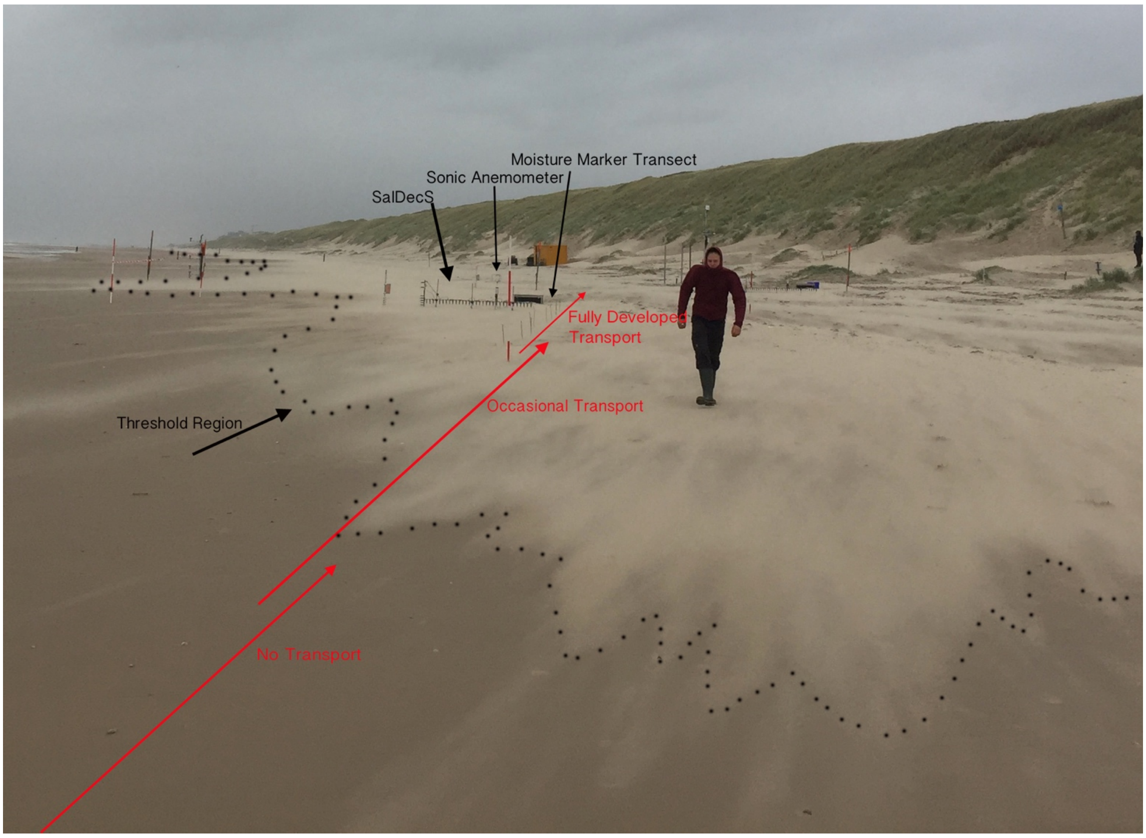

Figure 3.11 Instrument set-up during aeolian activity. Note the moisture marker transect perpendicular to the Saltation Detection System and the dashed threshold region of interest. At the moment the picture was captured, the threshold region was shifted seaward of the moisture transect, on such instances no moisture conditions around the entrainment threshold could be obtained. However, the geometry and location of this region appeared highly variable (see Figure 3.10 for a close-up of the moisture marker and SalDecS set-up).

In attempt to find a moisture and wind speed dependent threshold, moisture measurements were conducted perpendicular to the SalDecS (section 3.4.4) and continued upwind until visually transport ceased. The region between two markers where visually transport happened and where no transport was visible is the threshold region of interest. In this manner, the first grain entrainment without impact of other saltating grains was aimed to capture for a particular moisture content and wind speed as measured at 0.9 m height with the ultrasonic anemometer (Figure 3.11).

Threshold conditions are investigated by analysing the obtained data in three different ways. Firstly, the influence of unsteadiness of the wind on the entrainment is investigated by determining the maximum wind speed (gust) during the minute of moisture observations where no aeolian transport was visible any longer. In this manner, the maximum wind speed for no transport was intended to capture. Additionally, the wind speed averaged over one minute, during the moisture observations where aeolian transport was still visible was determined, in this manner the minimum wind speed for aeolian transport was aimed to capture. Furthermore, the middle between two subsequent soil moisture and wind speed observations that showed 'visual aeolian transport' and 'no visual aeolian transport' was determined. For these methods both the one-minute average wind speed around the moment of 'threshold moisture observations' (in the last two mentioned methods) and the maximum wind speed as measured in a block of one minute was used (in the first method). Measurements during aeolian activity were done on October 6, 11, 20, 25 and 29.

Field observations are compared with equations of Bagnold (1936), that uses the Shields parameter, and D_{50} to calculate the shear velocity threshold (u_{*t}) for static conditions and equations of belly (1964) that uses a logarithmic equation where u_{*t} is related to moisture content (w) resulting in a wet shear velocity threshold (u_{*tw}). In order to relate the wet shear velocity threshold (u_{*tw}) to wind speed, the 'Law of the Wall' is used with a roughness length set to $z_0 = D_{50}/30$. In this manner, the moisture content is related to the wind speed at which theoretically first entrainment of particles takes place.

Sampling method 3

In sampling method 3) moisture measurements are conducted in a 2 by 2 m grid consisting of 20 points that captured the edges of a sandbar- and trough system. This method was carried-out to assess the along shore surface moisture variability and influence of the morphology on the surface moisture content. The grid was sampled as soon as the falling tide allowed, the measurements were continued until the grid inundated again. In this manner surface drying and subsequent wetting of the morphology units was aimed to capture. The grid measurements were carried-out on the 26th of October.

3.4.2 Sea Surface Elevation

In aeolian studies the width of the beach is an important factor that controls the available fetch distance. The North-Sea water level, refers to the resulting water level variation due to the astronomical tide, wave and wind conditions which together with the geometry of the intertidal beach mostly determine the inundation level of the beach.

During the field-study the water level variations are registered by a pressure transducer referred to as the 'OSSI' (Ocean Sensor Systems International). The sensor was located on site at the shoreline around mean sea level, see Figure 3-9. The location of the OSSI was later assigned as the origin of the local coordinate system, which will be further explained at the end of this chapter (3.4.5).

Pressure time series were captured by the OSSI during the whole field-period at a frequency of 5Hz. The processed signal (processing includes an atmospheric correction and smoothening of the signal for consistency with the GW levels) gives the water level with respect to NAP (Normaal Amsterdams Peil). The processed signal of the OSSI is referred to as the Sea Surface Elevation (SSE) given in meters with respect to NAP.

3.4.3 Groundwater Fluctuations

Landward of the OSSI a cross-shore transect of six groundwater wells was installed in order to measure the temporal and cross-shore variations of the water table in the beach. The spacing between the wells ranged between 10 and 20m (see Figure 3-9). During the storm of October 6, the four most seaward located wells almost toppled over and one of the sensors was destroyed, after this event a new transect was installed on the October 9 of which only sensors in wells 3, 5, 6, 7 and 8 continuously measured over the remaining study period (see appendix I for operating periods, sensor types, sensor NAP values and locations)

The wells varied in length depending on the expected depth of the water table at location. This holds that the most landward well was installed deeper into the beach compared to the more seaward located wells (Figure 3.9). The surface of the water in the well will by definition be at atmospheric pressure (Horn, 2002) and give the position of the water table in the sediment around the location of the well. In order to transform raw pressure measured by the transducer to water levels w.r.t NAP a few field-calibration steps are performed.

Firstly, P_{total} as measured by the transducer in the well is corrected for the atmospheric pressure at that time instance (t) and for each of the wells (x) (equation 3.1). The resulting pressure ($P_{groundwater}$) will be due to groundwater alone. Then, using equation 3.2, and assuming hydrostatic conditions the height of the water column (η) is calculated using the gravitational acceleration (g) and density of the seawater (ρ). Location x refers to the cross-shore distance in meters, positive landward.

$$P_{groundwater}(t,x) = P_{total}(t,x) - P_{atmosphere}(t) \qquad (3.1)$$

$$\eta = \frac{P_{groundwater}}{g.\rho} \qquad (3.2)$$

The pressure transducers in the groundwater wells and the OSSI were calibrated in the laboratory before deployment. The pressure transducers measured the depth of the water table every 5 minutes, generating a time-series of the groundwater table elevation. This frequency is sufficient to measure groundwater oscillations caused by the tides.

In order to examine the cross-shore variation in tidal amplitude and phase, the timing and magnitude of the high and low-water levels for all wells were identified. The amplitude is defined as the tidal range (peak HW minus subsequent peak LW) divided by 2, as well as the mean amplitude at each well location was calculated. For this analysis, the offshore measured tidal water level was used, since the OSSI did not capture the timing and magnitude of all low water levels that occurred during the field period. The resulting gaps in the time-series emerged because the sensor was located slightly above the low water line on some days. The offshore water level measurements showed a time-offset (of about 15 minutes) with respect to on-site (OSSI) registered water levels. However, the magnitude of the oscillations was found equal to the onsite measured magnitude and could therefore be used in the amplitude calculation.

Furthermore, after identifying all the peak water level timings in the OSSI and well signals, the groundwater phase lag with respect to the tide can be identified, which is defined as the time-difference between an on-site OSSI registered peak and subsequent groundwater peak. Due to the discussed gaps in the OSSI time-series the subsequent phase-lag analysis is based on timing of the high-water levels only.

3.4.4 Saltation Intensity

During the field-campaign measurements of saltation intensity were conducted using the previously mentioned SalDecS, that acoustically measures the amount of sand grains colliding with a transect of 32 sensors employed perpendicular to the dominant wind direction at a frequency of 10Hz. The sensors are spaced at an interval of 0.10m making for a 2.40m wide transect including 8 vertically distributed sensors (Figure 3.11). For more information on the operation principles the reader is referred to de Winter *et al.*, (2018). Data on the wind speed as measured by the co-installed ultrasonic-anemometer is synchronised with the saltation data.

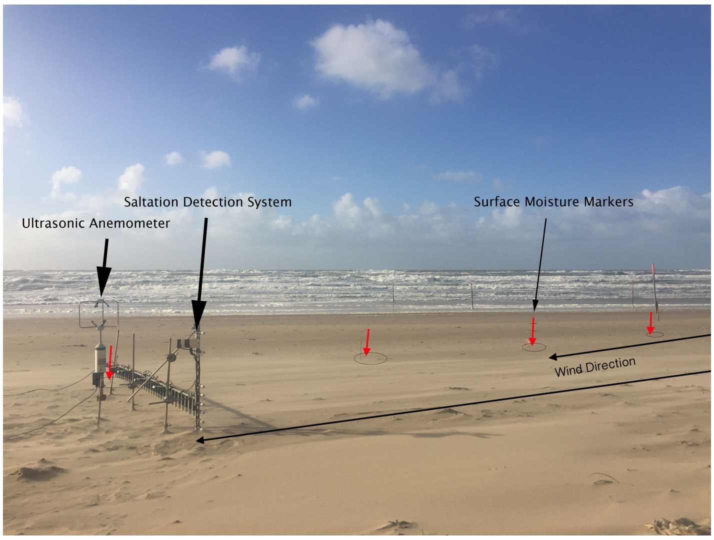

Figure 3-11 SalDecS, Sonic Anemeter and Surface Moisture markers, set-up on October 29.

The signal of the SalDecS is processed via the following equation (Equation 3.3), adapted from de Winter *et al., (2018).* The total number of particles counted during an experiment was divided by the duration of the experiment t (in seconds) to obtain the saltation intensity.

$$I = \frac{\sum counts}{t} \qquad (3.3)$$

With I the saltation intensity (counts s^{-1}).

3.4.5 Miscellaneous Measurements

To determine cross-shore variation in the grainsize distribution 15 sediment samples were taken along the groundwater well transect from the surface of the beach. The samples were analysed in the laboratory using 22 stacked sieves with apertures ranging from 2000 to 45µm. Results of sieving and subsequent granular analysis using GRADISTAT are displayed in the results section. Mean grainsize measures are composed after Folk and Ward in metric units, which provide the most robust basis for comparison of compositionally variable sediments (Blott and Pye, 2001).

The thickness of the capillary fringe is estimated along the same 15 cross-shore locations using two different equations (Equation 3.4 and 3.5) following Artherton, Baird and Wiggs (2001).

$$h_c = \frac{4\gamma\ cos\alpha}{d_m \rho_w g}$$ (3.4 after Dingman, 1984)

$$h_c = \frac{10\gamma}{d_m \rho_w g}$$ (3.5 after Turner and Nielsen, 1997)

Where h_c [m] is the thickness of the capillary fringe, γ the surface tension of sea water (taken 74 n/m, after Nayar et al., 2014), α the contact angle between water in a pore and pore side wall (taken zero), d_m is the mean grain diameter and with ρ_w density of seawater and g the gravitational acceleration. Mean grain diameter d_m is calculated after the Folk and Ward method in GRADISTAT (Blott, 2010) and can be used in (equation 3.3 and 3.4) instead of D_{50} pore radius (Dingman, 1984). Note that with $\alpha = 0$, h_c becomes 2.5 times larger using the Turner and Nielsen (1997) method. These methods are used to indicate a range of possible capillary thickness estimates as was found by Artherton, Baird and Wiggs (2001).

Locations of the moisture markers, groundwater wells and all other locations were determined using a Trimble RTK-GPS. RTK fix was realtime established by using services provided LNRnet; an independent GNSS network that provides RTK corrections up to 1cm accuracy. This network made the use of a radio connected base-station redundant during the field-campaign. Once RTK fix is established the GPS captures x, y and z coordinates with an accuracy of around $\pm$ 2cm. The beach profile was captured using the same RTK-GPS unit using a continuous measurement option. This option performs an x, y and z measurement every second. By using the GPS-unit located on a measuring wheel and holding it vertically level, the beach profile was captured by walking along the groundwater transect every day, see Figure 3.1 (lower right panel).

The slope (S) of the beach was numerically calculated by iteratively dividing the horizontal run length $(x_2 - x_1)$ by vertical rise height $(z_2 - z_1)$ for every 8th (xyz) gps-point from the profile measurements (equation 3.3).

$$S = \frac{x_2 - x_1}{z_2 - z_1} * 100\%$$ (3.6)

The RD2008 coordinate system used in the Netherlands was transformed to a local grid. For Moisture measurements along the well transect translation of the system was performed such that the origin is positioned at the location of the OSSI. Rotation of the RD2008 system (with positive x pointing East and positive y pointing North) is 8.32 degrees clockwise to obtain a local grid with the positive x-axis pointing cross-shore, landward along the groundwater well transact as in Figure 3.9. A similar approach was employed to create a local coordinate system for moisture measurements in front of the SalDecS, where translation and rotation of the RD2008 system was performed such that the first moisture marker at edge of the SalDecS corresponds to the origin, positive x points up-wind w.r.t. the origin.

4. Results

In order to assess the presented research questions (Question 1AB and C) firstly the cross-shore spatial variation during the study period is investigated (Section 4.1) after which properties of the groundwater oscillations are discussed and related to the tidal cycle (Section 4.2). In the subsequent section (4.3) the cross-shore spatial and temporal variation in surface moisture content in relation to the tidal cycle and subsequent groundwater fluctuations are discussed. Section 4.4 concerns next to the cross-shore also the along-shore variability and influence of morphology on temporal and spatial variation of moisture content. In section 4.5 more extreme environmental conditions are discussed with emphasis on the influence of storm-surges on the moisture variability. To tackle the second research question (Question 2A) results of particle entrainment thresholds are presented and threshold wind speed observations are related to surface moisture content.

4.1 Spatial Surface Moisture Variation

After calculating of the gravimetric moisture content from output of the Delta-T Theta probe, measurements of all 8 days along the well transect are plotted against the cross-shore distance (Figure 4-1A). The figure shows an overview of all moisture measurements obtained during 8 days. With investigating the figure, some general characteristics of the cross-shore spatial moisture distribution become apparent. Based on the moisture measurements and cross-shore distance, the beach is classified in lower- (0 - 45m), mid- (45 to 75m) and upper- (75 – 110m) beach. The beach parts are described and classified in terms of their moisture conditions as observed during the field-period, with classes; dry (0 - 5%), intermediate (5 – 17%) or wet (17-25%).

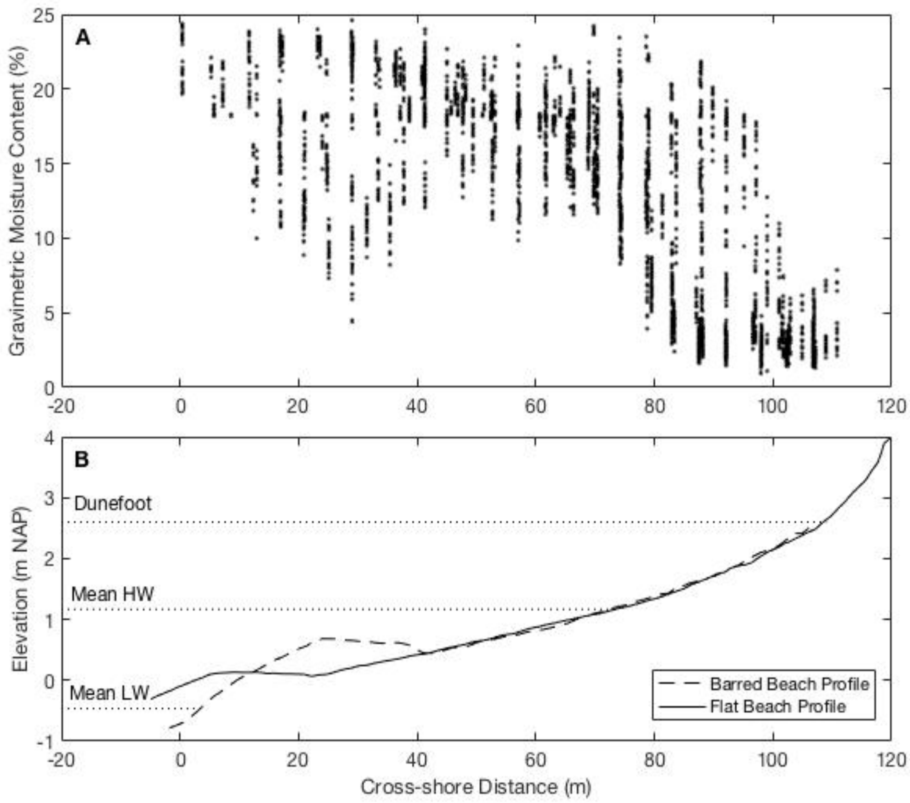

Figure 4-1 A) Spatial soil moisture variability during the field period, consisting of 4320 measurements. B) Beach profiles with and without intertidal sandbar, indicated are the dune-foot and mean high- and low tide as calculated from water levels as measured at the nearby IJmuiden buoy.

The upper-beach is characterised by mostly dry (0 - 5%) moisture conditions, especially at the higher parts of the upper-beach (and dune-toe) only occasionally intermediate moisture levels are encountered.

The mid-beach never reaches the dry moisture conditions as observed at the upper beach and wetness is always intermediate to wet. The mean high-water line dissects the dry upper-beach and intermediate to wet mid-beach, indicating that seaward of the mean high-water level at the mid-beach moisture conditions never became dry. However, on occasions when the lower-beach is characterised by the presence of an intertidal sandbar, moisture conditions may become dryer than the mid-beach, interrupting the general seaward increasing moisture gradient. The beach near the mean low waterline is always characterised by (near) saturated conditions.

Some statistics of the different beach-parts are given in table 4-1. Showing that the variation (standard deviation) is largest for the lower-beach and smallest for upper-beach. The upper-beach is distinguished from the other beach-parts by the much smaller mean moisture content.

Table 4-1 Mean, Standard Deviation, Range and Number of observations of the different beach parts

	Mean [%]	*SD [%]*	*Range [%]*	*No. Obs.*
Lower-beach	18	11	4-25	960
Mid-beach	18	8	10-24	1140
Upper-beach	8	9	1-24	2205

4.2 Tides and Groundwater

In order to explain the observed moisture variation some characteristic features of the groundwater table fluctuations are described and quantified. Figure 4-2 shows the time-series of water levels as measured by the 'OSSI' and groundwater wells of six subsequent days during both spring tide (A) and neap tide (B). The figure shows the oscillating nature of all the signals, associated with the semi-diurnal tidal oscillation in Egmond aan Zee. Also, note the cut-off OSSI signal during neap-tide low waters as discussed in the methods section. Furthermore, a slope (overheight or super-elevation) in the groundwater table is present. Most of the time the groundwater table slopes seaward, as landward wells measure higher water levels during the entire tidal cycle. Only occasionally on some specific parts of the beach the slope is inverted, with higher water levels at the seaward side. This generally happens during one hour around high water during spring tide, between the two most landward located wells.

Furthermore, as reflected by the time-series an important feature is the amplitude of the semi-diurnal oscillation of the groundwater table forced by the tides. The amplitude of the oscillations dampen in the more landward located wells. During neap tide the semi-diurnal oscillation in well 8 is most completely diminished (panel B Figure 4-2), while the oscillation is still apparent during spring tide (panel A). Having a closer look at the timing between peaks and troughs in subsequent wells it is found that a time-offset in the signal between well 7 and 8 and the more seaward located wells (and OSSI) exists. Furthermore, it becomes apparent that the timing of high water as measured with the OSSI and the peak in groundwater level in well 3, 5 and 6 is equal.

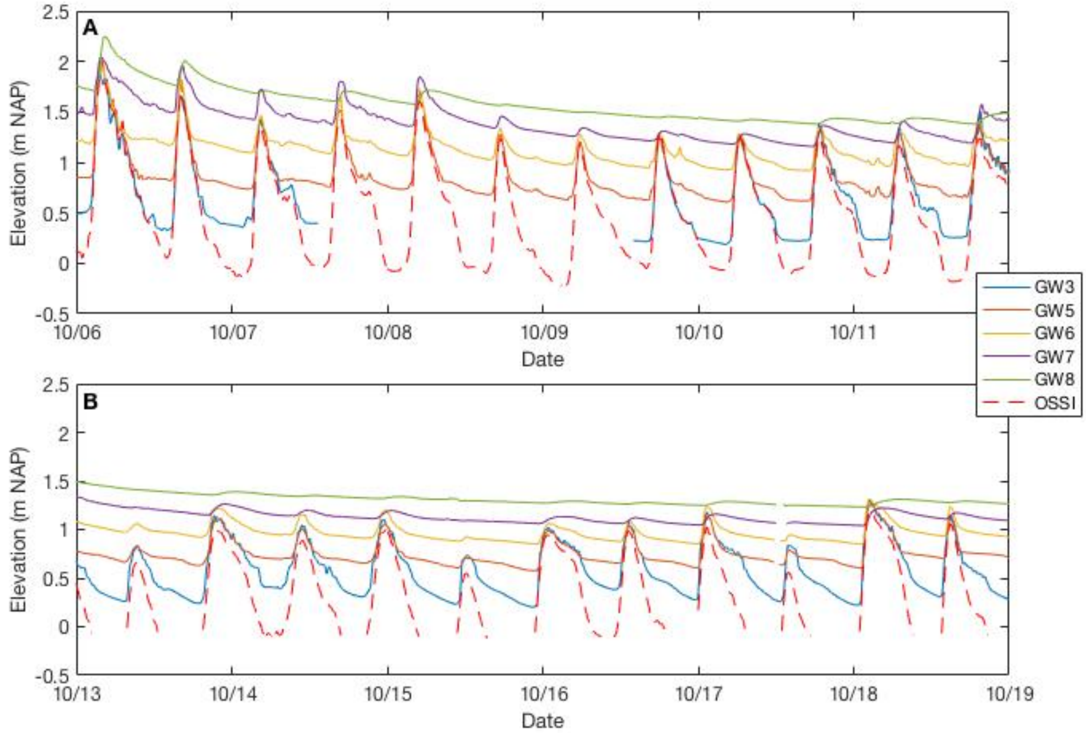

Figure 4-2 Water level time-series as measured by the 'OSSI' and the pressure transducers deployed in the cross-shore transect of groundwater wells during A) spring tide on October 6 onwards and B) neap tide on October 13 onwards.

The transformation of the tidal signal as it propagates into the beach is further investigated and quantified, see the following figures, 4-3AB and 4-4AB. As previously noted, decay of the semi-diurnal groundwater level amplitude in the cross-shore direction is observed. The mean semi-diurnal amplitude as registered by the OSSI is about 0.75m were GW8 registered a mean oscillation of only 0.04m. Investigating the landward evolution of amplitudes reveals that the it decays exponentially moving landward. Investigating the trend from as seen in the figure it is expected that influence of the semi-diurnal tidal oscillation on the groundwater signal is diminished some 15 meters landward of GW8, well into the dune-foot. Furthermore, the indicated mean high-water level suggests that on average during the field period well 6 was located just slightly above the waterline. This observation has been taken into account in the next phase-lag calculation, which was not present in well 6 even during neap tide.

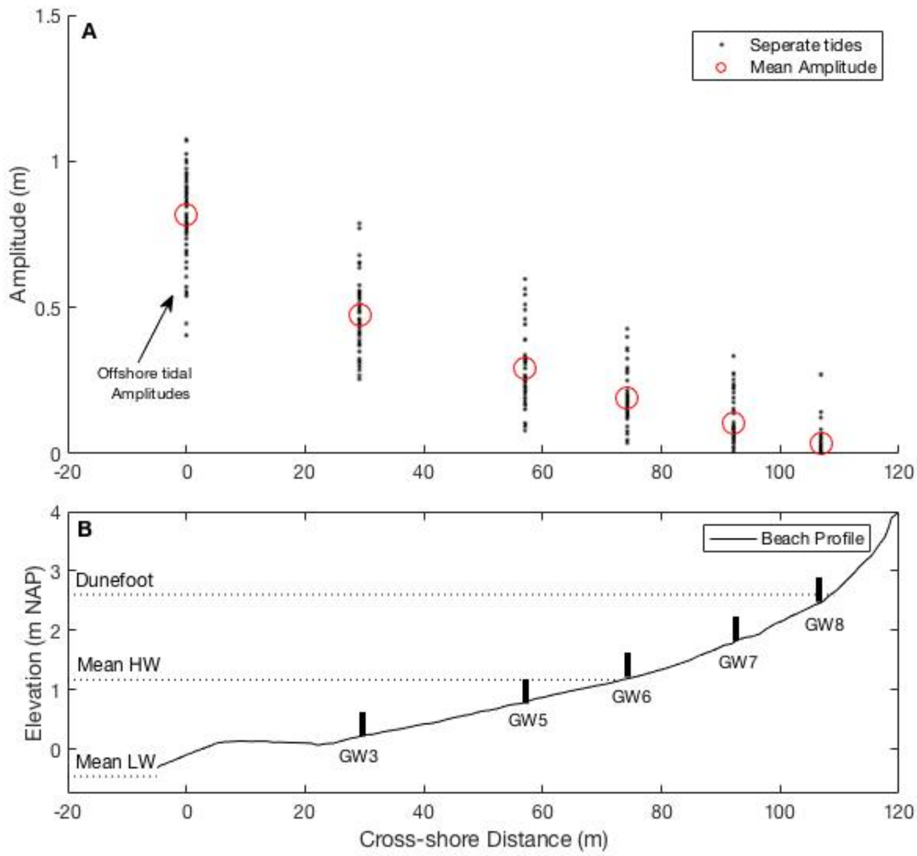

Figure 4-3 A) Cross-shore evolution of amplitudes and B) High water phase-lag evolution of well signals with respect to SSE.

Transformation of the oscillating tidal signal in the beach is further investigated by looking at the time differences between maxima of the OSSI registered water levels and the groundwater table elevation, see the following Figure 4-4AB. Wells 7 and 8 indicate an increasing phase-lag at the landward located wells. The largest phase-lag with respect to the tide is 335 minutes in GW8, indicating that although tidal elevation is already approaching low-water, groundwater levels are still adjusting to the previous high-water. Furthermore, the figure shows that the largest high-water phase-lag happens on occasions when watertable elevation in well 7 is larger than in well 8. Furthermore, the spring-neap cycle seems to influence the high-water phase-lag. With a smaller phase-lag of about 50 minutes during spring tide (around October 8) and larger phase-lag of about 150 minutes during neap tide (around October 15). The trend does however not continue during the next spring cycle (around October 22) where the phase-lag is larger than during the previously observed spring cycle. At the end of the time-series during the next neap cycle (around October 29) the phase-lag is similar to the previously observed neap phase-lag.

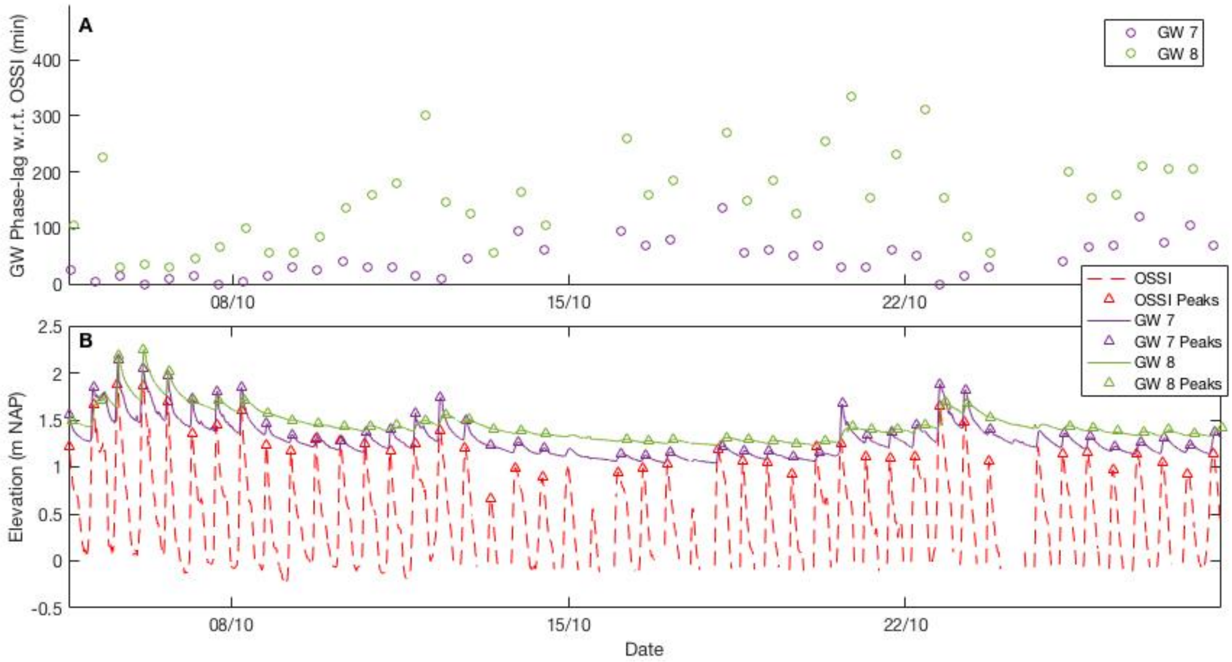

Figure 4-4 A) Phase-lag between peak water levels of the groundwater signal at well 7 and 8 with respect to previous OSSI-measured peak. B) Time-series of OSSI and wells, indicated is the timing of peaks on which the phase-lag calculation is based.

From the previous analyses became apparent that groundwater fluctuations are linked to tidal fluctuations, the groundwater table oscillates at the same frequency as the tide but properties and timing of the oscillations change. Differences between tidal water level and groundwater level include: the presence of overheight, the amplitude of the oscillations decrease in the landward direction and the highwater phase-lag increases in the landward direction.

4.3 Tides, Groundwater and Temporal Surface Moisture Variability

Figure 4-5 shows the groundwater table and the surface moisture content as measured at the beach surface around the indicated wells on October 24, during spring tide. During this day moisture measurements were continued from approximately high water in the morning (6:30), to low water in the afternoon (15:00), until the next high water in the evening (18:05). Note that the left y-axis indicates the depth of the groundwater table below the surface. Thus, increasing positive values indicate a falling groundwater table below the beach surface and negative values indicate a water level above the surface of the beach. The figure reveals that the groundwater table is falling during most of the time when the moisture measurements were conducted. The surface moisture as measured at the four wells show a corresponding drying trend during the day, with the exception of some measurements at the end of the day when the groundwater table started rising again. The inundation level due to the tides allowed more moisture measurements at the landward located wells compared to the seaward located wells.

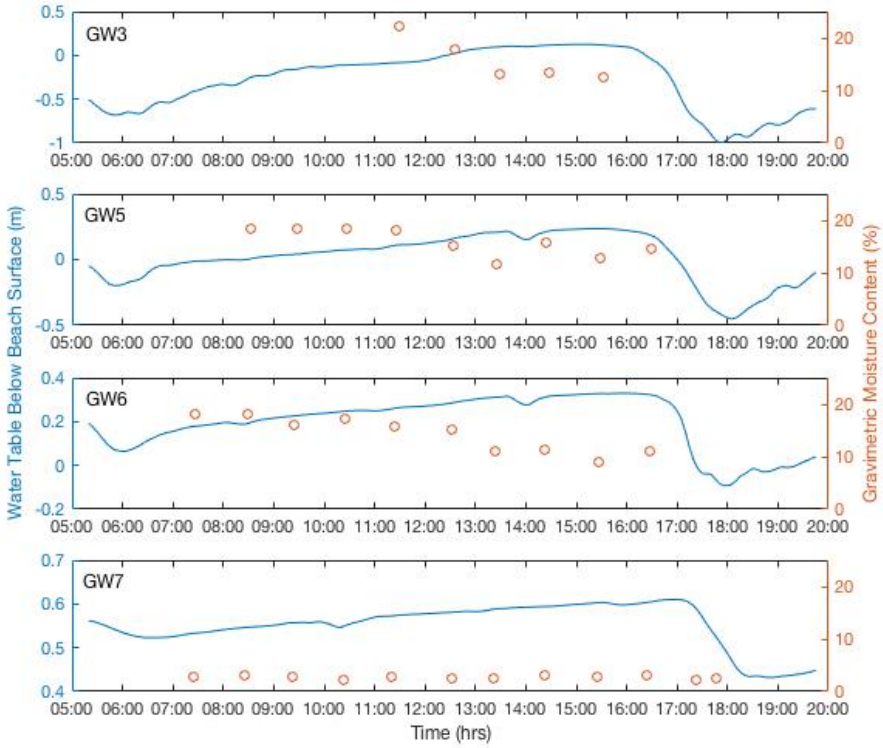

Figure 4-5 October 24, time-series of groundwater table depth (left y-axis) and measurement points of surface moisture content at the indicated times (right y-axis). High tide was 6:30 in the morning, next low tide was 15:00 and the subsequent high tide around 18:05.

At well three (upper panel) the depth of the groundwater table increases from -0.08m to 0.12m, with corresponding moisture content decreasing from 22.3% to 12.5%. The negative groundwater depth indicates a water level above the beach surface, which seems contradicting since surface moisture was still obtained at the beach at this time. An explanation could be that the moisture measurements were conducted in between wave run-up excursions, that averaged over 5 minutes made for a water table above the surface of the beach. The second two panels show a similar trend, with increasing water table depth resulting in subsequent surface drying of the beach. At well 5 (second panel) the decreasing groundwater table depth between the moisture measurements with the largest desiccation (as measured around 8:30 and 13:30) is from 0.01m to 0.21m with surface drying from 18.3% to 11.6%. At well 6 this holds a decrease from 0.18m to 0.33m with surface drying from 18.3% to 9.0%. It is interesting to see that moisture conditions at both of the wells at the start of the measurements were 18.3% but that the difference in groundwater table depth is quite large (0.17m). Indicating that even though the phreatic surface is well below the beach surface, capillary water still moisturises the surface up to saturated conditions. At well 7 the surface moisture does not show any significant response to the drop in the groundwater table, since the watertable is situated quite deep (between 0.53m to 0.61m) below the surface.

The directly linked response between surface moisture conditions and watertable depth becomes clearly apparent at 14h00 where the watertable rises for an instant while it was generally dropping with the falling tide, as reflected by the bump in the signal in well 5 and 6. At this time, the surface moisture content around these wells reveal a sudden and slight increase in wetness during the general drying trend. This wetting response in surface moisture is stronger at well 5 where the watertable is closer to the beach surface, a watertable rise of 0.06m (from 0.21m to 0.15m) results in an increase of 4.2% moisture content (from 11.6% to 15.8%).

In the following figure (Figure 4-6) data of October 26 is displayed with the x-axis denoting the cross-shore distance (m), and y-axis showing gravimetric moisture content (%) (upper panel) and elevation of the beach profile and watertable (m) with indicated well locations (lower panel). The general spatial moisture distribution that emerges is characterised by a seaward increasing gradient. An exception is the intertidal-sandbar at the seaward edge that shows intermediate moisture conditions as observed in the last two measurement runs. The temporal variation as observed during this day is characterised by drying between the runs at the mid- and lower-beach. The upper-beach shows no variation, similar as was discussed in the previous example during a watertable relatively deep below the beach surface. Drying only occurs at locations that were wet at the start of the day, followed by a falling groundwater table.

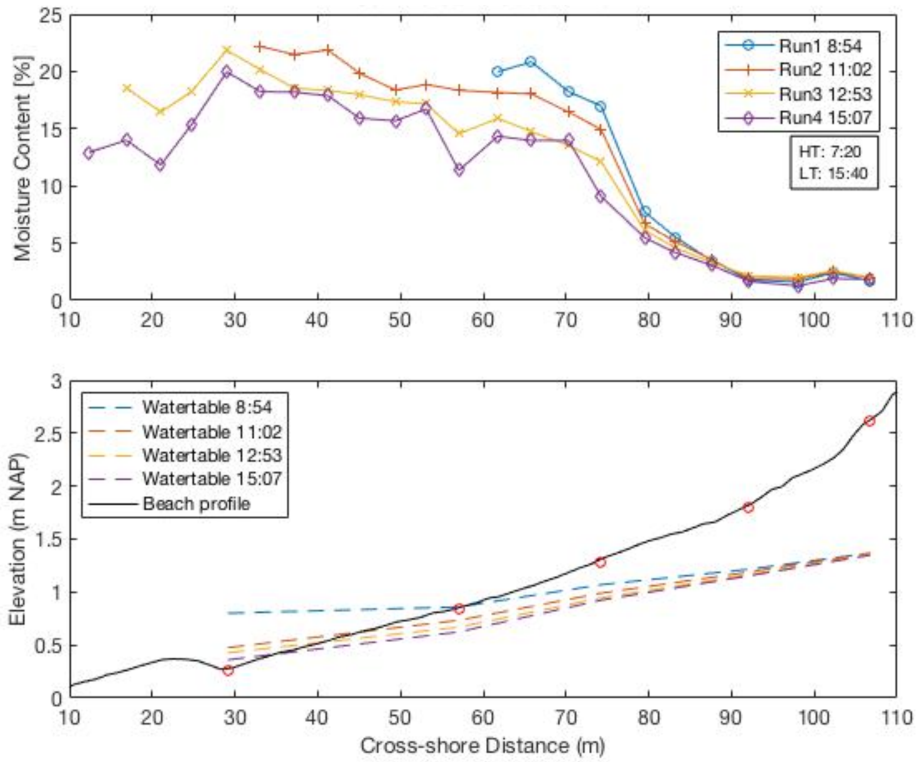

Figure 4-6 October 26, cross-shore variability of the surface moisture as measured during 4 different runs towards low-tide (upper panel) and watertable elevation (lower panel) during the different runs. Indicated are also the beach profile and locations of the groundwater wells.

The following figure (Figure 4.7) displays the data of October 24 which clearly reveals drying of the surface as was previously discussed for this day. However, with displaying the same data as a function of the cross-shore distance the drying trend over the entire beach is clearly revealed. Also, the falling watertable associated with the falling tide between run 1 and 4 is clearly present. The surface moisture distribution is characterised by a large cross-shore spatial gradient, from 18.2% to 3.0% between x = 75 m and 92 m. The location of the gradient remains present during the day but it's magnitude decreases slightly, associated with 6hrs of dryings during the falling tide and subsequent dropping watertable. The spatial gradient diminishes seaward of x = 75 m, and rather spatially uniform drying between the first four runs is observed. This uniformity corresponds to a slope in the groundwater table that is similar to the slope of the beach during this day.

Furthermore, examining the last three runs reveals that the beach becomes wet with tidal inundation in a rather short time, (in approximately 3hrs) compared to the slower drying (in approximately 6hrs). Comparing run 4 and 5 reaveals that surface wetting takes place some distance (about 15m) in front of the wave run-up excursions (moisture measurements are continued up to the wave run-up limit), with an offshore wave-height measured around 1m during this day. Furthermore, note the inversed slope of the groundwater table during the last measurement run as was discussed in the previous section, which makes for a large spatial gradient in the surface moisture distribution around this time, with dry conditions only some 6 m landward of the saturated conditions near the wave run-up limit.

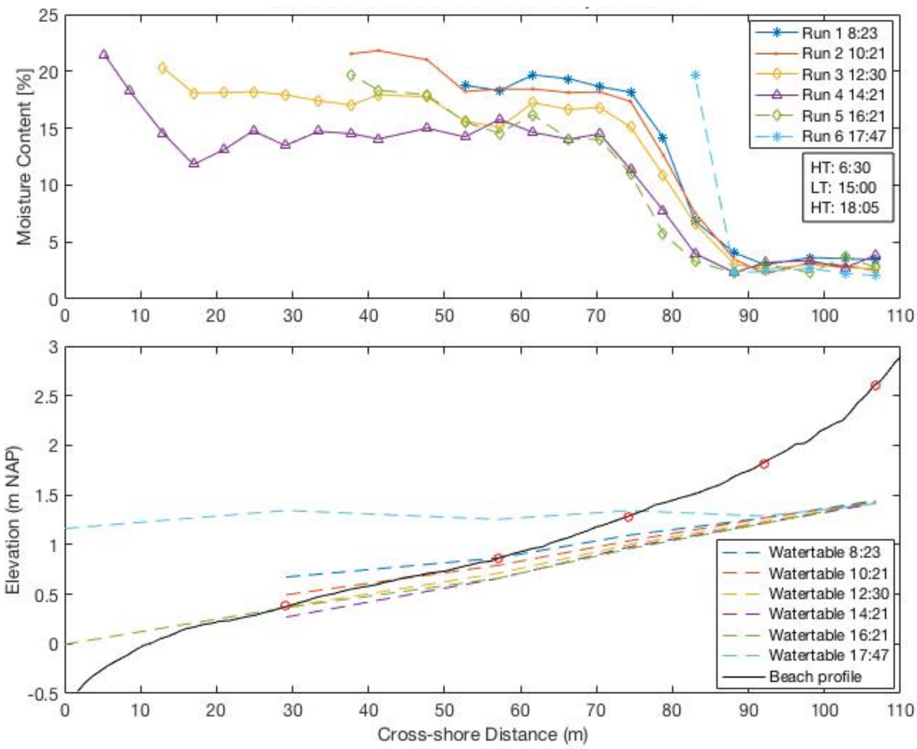

Figure 4-7 October 24, Cross-shore variability of the surface moisture as measured during 6 different runs (upper panel) and watertable elevation (lower panel) during the different runs. Indicated are also the beach profile and locations of the groundwater wells.

The following figure (Figure 4-8) concerns the surface moisture conditions as observed during neap-tide on October 16. Measurements were started one hour before low-tide at 10h. Most of the beach shows a rather constant moisture distribution, temporally speaking. The only drying of surface emerges at the sandbar, until subsequent inundation. On this location, between the first two runs the groundwater table is still adjusting to the low-tide level as reflected in the lower panel of the figure. The temporally steady moisture conditions on the mid- and upper beach during the first three runs are explained by the steady depth of the groundwater table. Spatially, the general seaward increasing moisture gradient is interrupted by the presence of the intertidal sandbar. Note that the slope of the groundwater table during this day is different from the slope of the beach (which is steeper). This explains the non-uniform moisture distribution, in contrast to observations of the previously discussed, more spatially uniform moisture distribution on October 24.

Wetting of the sandbar happens as soon as the tide, with superimposed wave run-up excursions inundate the bar, rapid gravitational drainage at this location might cause a temporally varying moisture distribution with frequency of beach inundation due to the waves. Which could however not be observed with the employed sampling frequency (hours). Wetting of the trough is observed after the tide starts to rise (run 3), which happens next to lateral inundation via the trough (field observation, not present in shown data) also via the rising groundwater table (Figure 4-8B). Wetting of the beach as reflected in the last measurement run (run 4) takes place some 10 m in front of the wave run-up excursions. During this day, the wave conditions were very calm with an offshore measured wave height of about 0.5m.

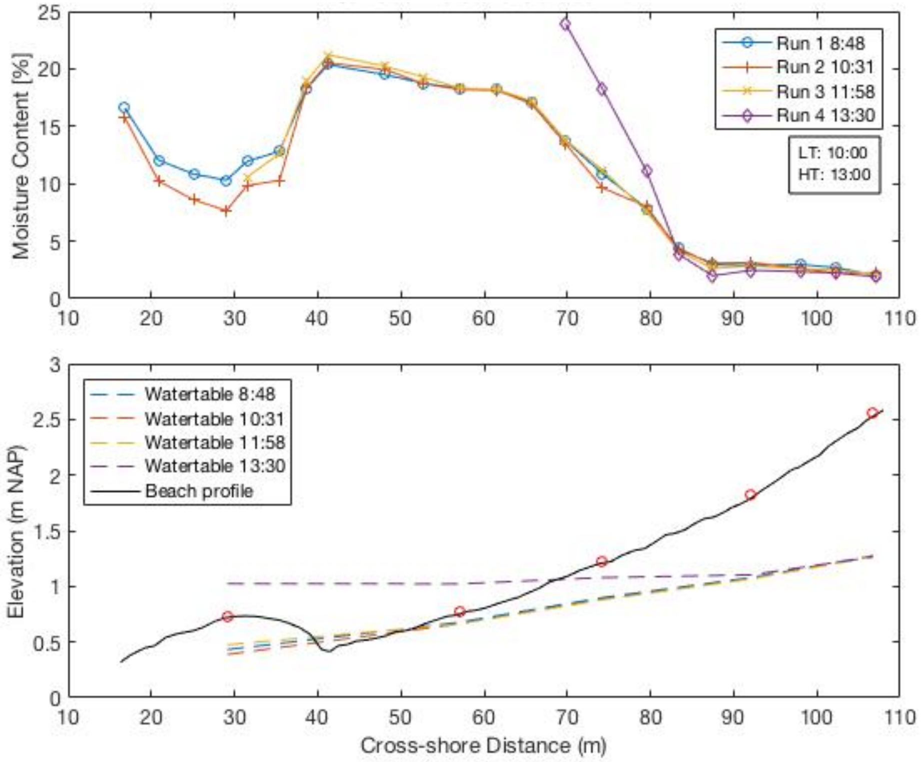

Figure 4-8 October 16, Cross-shore variability of the surface moisture as measured during 4 different runs (upper panel) and watertable elevation (lower panel) during the different runs. Indicated are also the beach profile and locations of the groundwater wells.

From the previous examples became apparent that the surface moisture content of the beach is highly variable in both space and time and a correlation between the depth of the phreatic surface and surface moisture content is present. Results showed that the cross-shore spatial variability bears different general trends. Including a cross-shore gradient, with dry conditions characterised by the residual water content at the dune toe and (over)saturated conditions near the waterline. However, the magnitude and distribution of the gradient varies per cross-shore location with each day. It was observed that a slope of the beach equal to slope of the water table results in rather uniform surface moisture conditions over the lower- and mid-beach. On occasions where the slope of the beach is larger than the slope of the phreatic surface (and the water table is within considerable distance from the beach surface) the observed gradient is distributed over a larger cross-shore distance. Furthermore, on measurement days where the beach was characterised by the presence of an intertidal bar, the general gradient was interrupted by dryer conditions at the bar.

Temporal variations showed strong resemblance with the tidal oscillations in Egmond aan Zee, with slow drying during tidal ebb-currents and a falling watertable and fast wetting during tidal flood-currents and a rising watertable. From the temporal variations became apparent that variations occurred in accordance with the variations in groundwater table depth. However, for saturated moisture conditions a range of groundwater depths (0 to 0.18m) was observed.

In order to evaluate the relation between the depth of the watertable and wetness at the surface based on field observations, every moisture measurement done at a groundwater well is plotted as a function of the watertable depth (Figure 4.9). To investigate influence of atmospheric processes, measurements that were done during highly evaporative conditions as calculated from the Makkink reference evaporation are indicated as well as measurements done during or after rainfall are indicated. Measurements obtained during overcast, non-rainy days with intermediate temperatures are indicated "neutral". The van Genuchten (1980) retention curve is fitted to the data, with fixed parameters the residual (1.5%) and saturated (18%) water content. The fitted parameters in the Van Genuchten equation (eq 2.3) return α = 3.1846, n = 5.4722 and m = 0.8173.

Figure 4.9 reveals that the measurements can be partly explained by the soil water characteristic curve. On the right side of the figure the residual water content (field capacity) of this sediment is present, holding 1.5% moisture with groundwater levels ranging from 0.5 up to 1.3m below the surface. On the left side of the figure the thickness of the capillary fringe may be read from the y-axis. Here, moisture conditions are saturated up to a watertable depth of about 0.2m, indicating the observed thickness of the capillary fringe as measured during the entire field campaign. With increasing watertable depths the surface moisture content rapidly decreases until some 0.7m where the sediment reaches the field capacity, the surface does not become increasingly dryer with further increasing watertable depths.

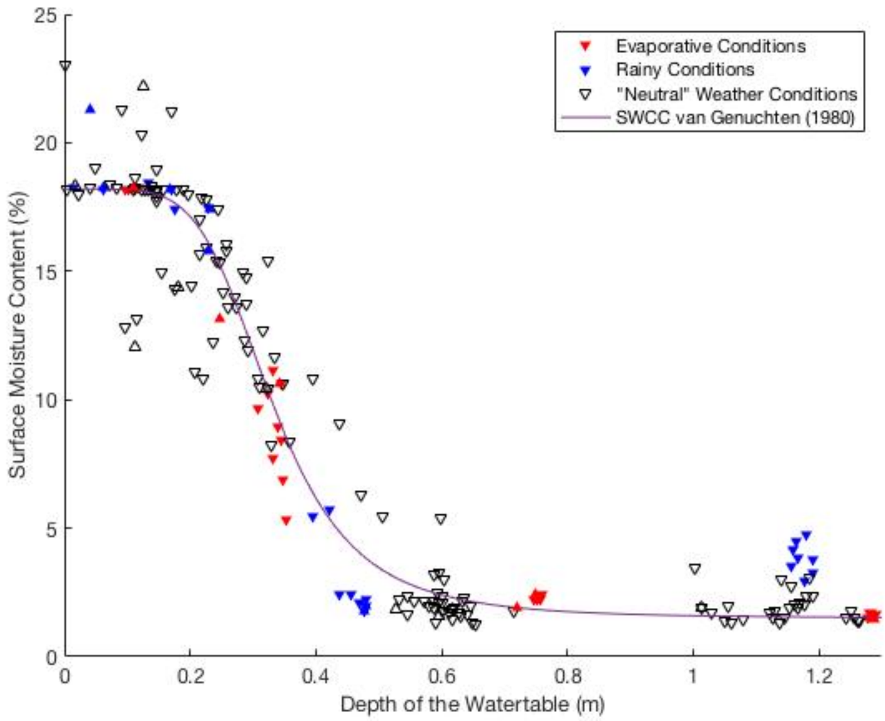

Figure 4-9 Surface moisture as function of groundwater table depth and a fitted Van Genuchten SWCC. Orientation of the triangles indicate whether measurements were obtained during a rising (upward pointing triangle) or during a falling (downward pointing triangle) watertable

Results of the grainsize analysis are used to theoretically predict the capillary fringe thickness using two different methods. Results are shown in figure (4.10). Dingmans (1984) method underestimates the observed capillary fringe, observations reveal saturated conditions with a watertable up to 0.2m below the surface while the thickness was estimated at 0.12m (averaged over the cross-shore variation). Turner and Nielsen's (1997) method overestimates of the observed capillary fringe thickness with cross-shore averaged 0.28m. These results suggest that the middle of the range as revealed by the different theoretical methods gives a good indication of the observed capillary fringe thickness as was found by other authors (Artherton, Baird and Wiggs, 2001). Implying that the beach remains saturated for watertable depths up to 0.20m below the beach surface.

During evaporative conditions (on October 16 relatively large Makkink reference evaporation was calculated from temperature and incoming solar radiation measurements) it is expected that surface moisture content is lower than during overcast and cooler conditions, for similar groundwater depths. However, no significant trend is visible, since during the warm and sunny day, moisture conditions for a certain watertable depth were not exceptionally low since the measurement do not organise more pronounced below the fitted SWCC. This suggests that capillary replenishment of moisture was sufficient to maintain the expected moisture conditions as predicted by the curve. It is worth noting that this is also true for the low moisture percentages in the range, where unsaturated water flow becomes slower with a reduced hydraulic conductivity. If dryer conditions were expected due to evaporation, it is in this region of the curve.

Obviously, during or after rainfall, surface moisture content is larger than during conditions without rainfall. However, not all measurements done during or after rainfall show significantly wetter beach conditions. With the exception of the measurements at the right side of the figure, where wet conditions prevailed during a relatively low watertable. These results suggest that groundwater processes are relatively more important in modulating the surface moisture content compared to atmospheric processes.

To investigate the in theory discussed hysteric behaviour of the surface moisture content, distinction is made between surface moisture data gathered during a rising and falling watertable. It is expected that during a rising watertable the surface moisture conditions are dryer compared to surface moisture conditions for the same water table depth during a falling water table. However, as the measurements suggest, no such trend is visible, since the amount of data points for a falling watertable lie below the curve as much as the measurements for a rising watertable do.

The results reveal the relation between the surface moisture content and the depth of the groundwater table and show that a parameterized SWCC can explain most of the surface moisture variability on a natural beach exposed to both marine, subsurface and atmospheric processes.

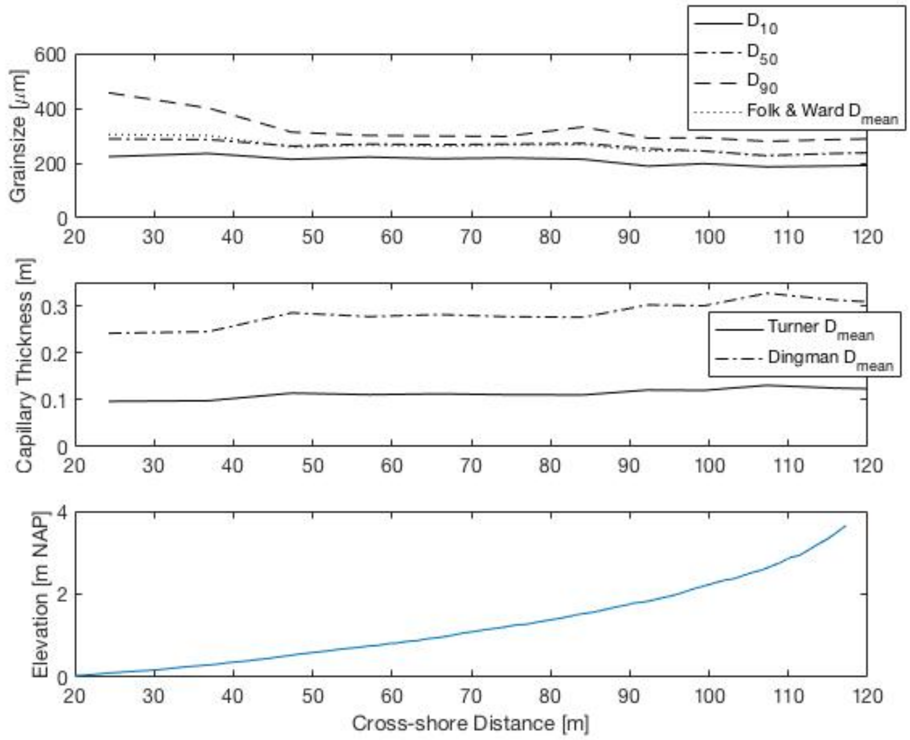

Figure 4.10 Sieving results (upper panel) with two estimations of capillary fringe thickness based on the grainsize (middle panel) and the cross-shore beach profile (lower panel) as measured during the day the grainsize samples were obtained.

4.4 Alongshore Surface Moisture Variability and Morphology

The following section elaborates upon research question 1B, concerning the influence of the morphology on the surface moisture content. From previous results became apparent that the presence of an intertidal sandbar tends to show more desiccation compared to other parts of the beach and that the slope of the beach plays an important role in modifying the cross-shore moisture content, this observation is linked to the finding that the depth of the water table below the surface of the beach is the most important control in modulating the surface moisture content. The relation between the two is best described by a fitted soil water characteristic curve based on the van Genuchten (1980) expression. In this section, next to the cross-shore variability also the along-shore spatial and temporal surface moisture variability is investigated in relation to the topography.

Kriging interpolation results of the grid measurements performed on October 26 are displayed in Figure 4-11. During this day, with the falling tide an inter-tidal sandbar and trough emerged that were sampled as long as the inundation level allowed. The upper left panel of the following figure shows the elevation in m NAP. The edges of the bar are up to + 0.4 m NAP in elevation and part of the sampled trough about + 0.05m NAP. The other panels show moisture content as measured during each of the 7 runs. Note that the scaling on the axis of the first moisture panel is different from the others (x and y axis denote 15m instead of 20m distance in the other panels). This is because the grid was still partly inundated at this time and a smaller grid was sampled, which in the later runs was extended as soon as the tidal level dropped sufficient.

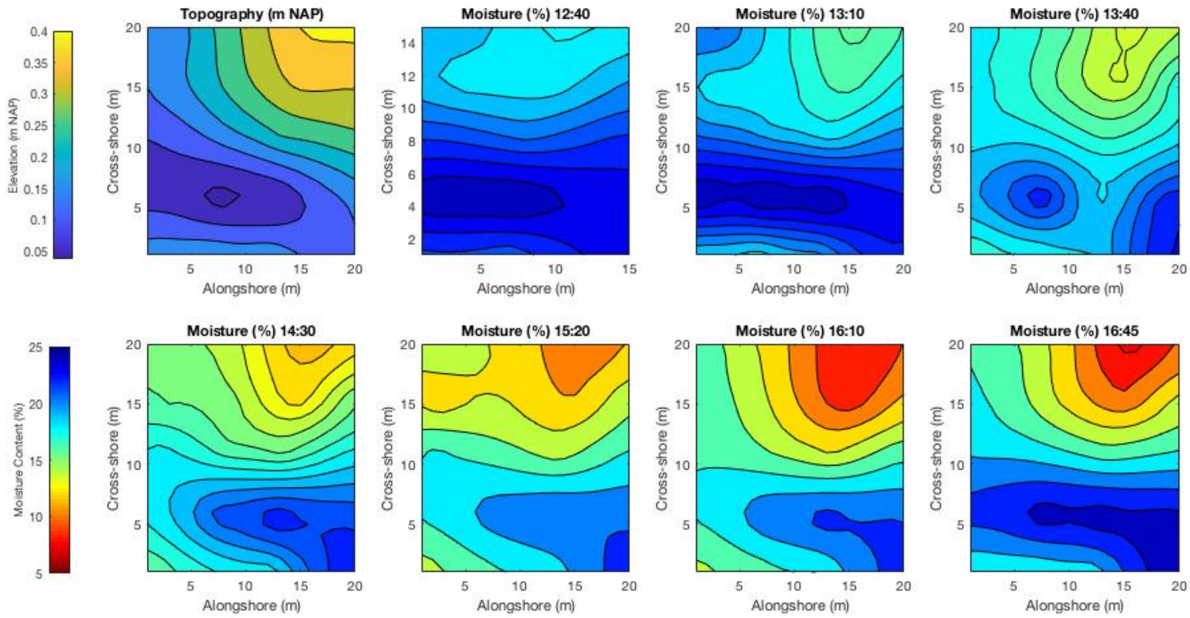

Figure 4-11 Interpolated grid beach surface elevation and surface moisture content. Upper left panel shows elevation w.r.t NAP, other panels show 7 moisture measurement runs at indicated time-intervals.

Apparent from the figure becomes that the higher parts in the upper-right corner of the grid show rapid drying; from 17% up to dry conditions (5% moisture) in some 3 hours. The trough remains saturated (>17% moisture) in all runs. However, some drying occurs as the tide continues to fall, but the rate of drying at the higher elevated parts is much faster. Once the water level starts to rise again (timing of low water is 15:40), lateral wetting of the shallowest parts occurs first, while the higher elevated bars continue to dry. The figure also shows that the variation in moisture content is strongly correlated with the topography of the beach. Suggesting that the groundwater table below the beach is a smooth surface that does not follow details of the morphology. These results are in line with the previously presented relation between depth of the groundwater table and surface moisture conditions. However, results showed that in addition to the cross-shore variation also along-shore variability in moisture content is present associated with the present morphology.

4.5 Storm-Surge Drying

The moisture measurements on the 6th of October were done after the storm surge of the previous day and night. The OSSI registered a high tide of 1.9m +NAP around 3h45 which (together with high water levels of the previous days, associated with surge and spring tide) resulted in an exceptionally high elevated groundwater table in the upper beach (note the elevated peak at the start of the time series shown at beginning of this chapter, Figure 4.2).

The following figure (Figure 4-12) shows an indent of the previously shown groundwater time-series. It shows the groundwater levels during the day after the storm-surge, October 6. Note the steady horizontal signal of well 4 and 5. At well 5 the steady groundwater level is registered at 1.232m +NAP, which corresponds to the beach surface height at this well, indicating the presence of a seepage face that was also visually observed during the moisture measurements this day. The arrow indicates the migration of the seepage face exit-point in between well 4 and 5. The migration of the exit point holds 17m in 1h45. This observation based on the well signals suggests that groundwater drainage from the upper beach was sufficient to maintain the groundwater table to such an elevation that it outcrops at the beach surface.

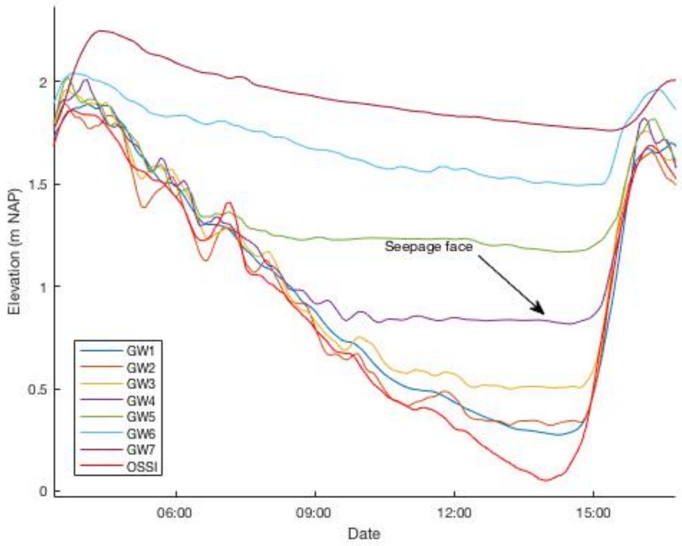

Figure 4.12 Groundwater level time-series as observed after the storm surge, indicated with the arrow is the migration of the exit-point between well 5 and 4.

The moisture measurements were done on the beach part that was not (over)saturated; from the dune-toe shoreward until just before the exit point, but not continued shoreward of the exit point with the exception of the most seaward located measurement of the first run, that was measured at the visually observed exit point indicated by the transition of a matte to glassy beach surface (Figure 4-13). Part of the beach that was not characterised by exfiltration indicated by the glassy, saturated beach surface was only some 25m wide and showed a drying trend during the 4 hours of measuring, corresponding with the falling groundwater table.

It should be noted that the location of the exit point based on the groundwater signal is different from the exit point observed in the field, because the pressure transducers deployed in the groundwater wells measure the height of the water table (Horn, 2002), disregarding the height of the capillary fringe that contributes to the exit-point location. Thus, discrepancies between a visually determined exit-point and an exit point based on the well signal might be present. It is expected that a visually observed exit point would be situated landward of a well-based exit point observation, which is in accordance with the presented observations.

The most important aspect of these observations is the fully saturated mid-beach, that was maintained until low-tide. The elevated groundwater table associated with the high Noth-Sea waterlevels due to the preceding storm-surge made for saturated conditions over the intertidal beach during low-water.

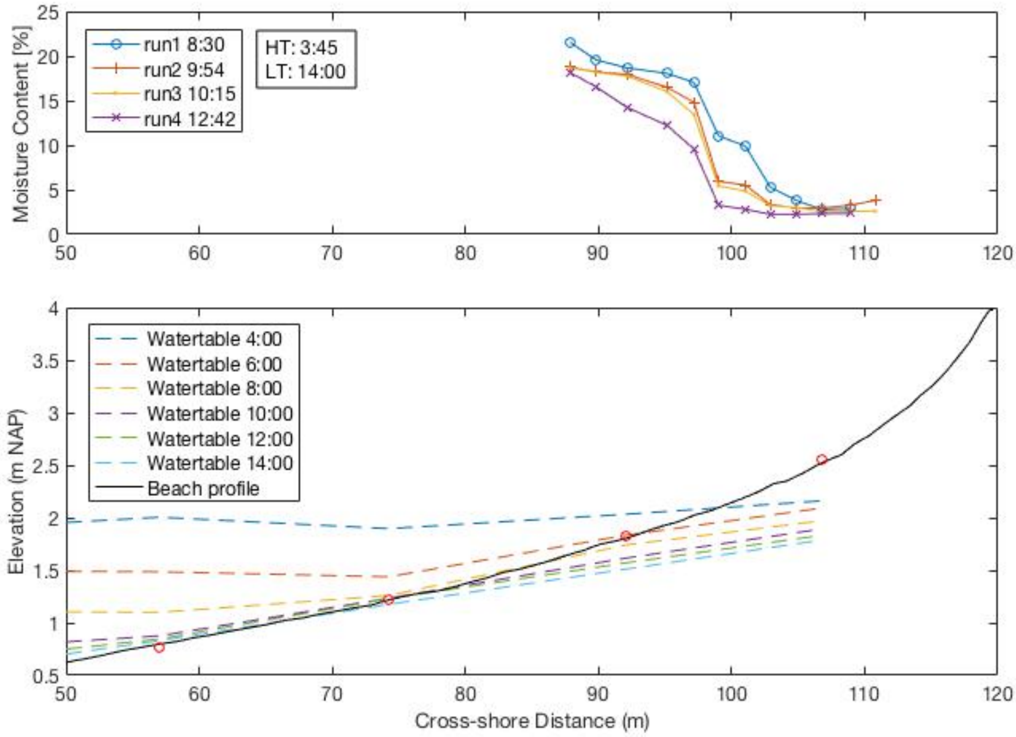

Figure 4-13 October 6, Spatial and temporal surface moisture variability of the upper beach after a storm surge, (upper panel). Corresponding beach profile and groundwater well locations with groundwater table elevation at indicated times, note that the adapted timing is not equal to timing of the moisture runs but has with a 2hr interval. Furthermore, note the muc smaller cross-shore distance compared to previously displayed figures.

4.6 Moisture and Wind Speed Dependent Grain Entrainment Thresholds

The second research question (2A) assesses how the surface moisture content alters the threshold for first aeolian transport. The possibility to determine a critical moisture content where above no entrainment takes place and where below aeolian activity starts for a certain wind speed is investigated. In literature, several values for a critical moisture content are presented. Delgado-Fernandez (2011) proposed the threshold at 10% moisture and Sarre (1984) proposed a threshold at 14%. However, also became apparent that a single value for a threshold condition was unable to account for the complexity as found on a natural beach (Cornelis and Gabriels, 2003). Results of visual entrainment threshold observations are presented in the Figure 5-11. Results of the moisture profiles obtained in front of a SalDecS on October 11 and the saltation intensity and wind speed are included in Figures 4-14A and 4-14B.

Analysis of a wind and moisture dependent threshold is based on the visually observed threshold cases. The upper panel in the following Figure 4-14 (Panel A) shows the relation between the moisture content and the maximum gust wind speed as measured at the time instance where no aeolian activity in the transect was visible anymore. The points in the figure suggest that for low moisture contents gusts are weaker to just not produce transport. During wet conditions wind gusts are stronger to not produce transport (note that in all instances transport was observed just one measurement location downwind of the displayed data point).

The middle panel (Panel B) bears the same structure, however, instances of first entrainment are displayed. The one minute averaged wind speed during observations of the last observed instance of aeolian activity in the transect was used (in this panel windward of the displayed observations no transport was observed anymore). Some resemblance with the previous figure is present, with a low threshold wind speed associated with dry conditions. Furthermore, grains on a wet beach are only released during stronger wind conditions. Interestingly, even during near saturated conditions (>15%) and high wind speeds (9 m/s) grains are released. Furthermore, it is interesting to see that wind speeds associated with gusts did not produce transport while one minute averaged wind speeds that lie below the gusts did produce transport. This inconsistency is further elaborated upon in the discussion section.

The last panel (Panel C) denotes the same axis, data points are plotted as the average between two moisture and wind speed observations, obtained from the last transport observation and the first no-transport observation. Furthermore, model results (Based on the presented equations of Belly and Bagnold) reveal the wet entrainment thresholds (shear velocity due to wind speed at 0.90m height) are displayed. Again, an increase in wind speed is observed for the first grains to be released but the relation is dominated by scatter.

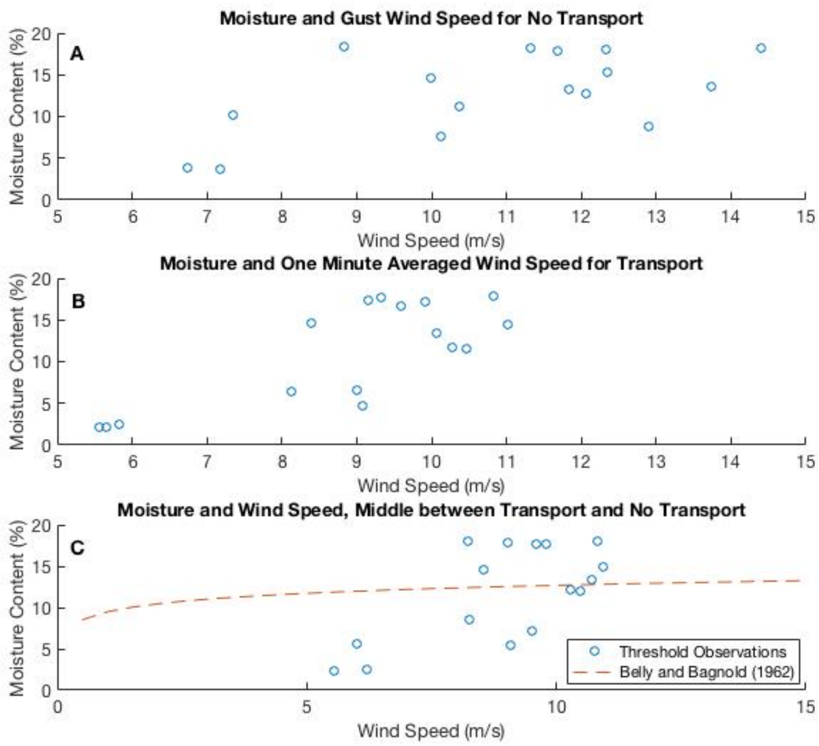

Figure 4-14 Three different measures of first particle entrainment based on visual field observations. Wind speed is measured at 0.9m. Modelled entrainment thresholds based on shear velocity calculations with equations of Bagnold (1936). Critical shear velocity is corrected for moisture content based on the equation of Belly (1962).

More results of moisture and wind speed dependent entrainment thresholds are given in the following figure. The moisture distribution in Figure 4-15A reveals a gradient in moisture content, upwind measurements show wetter conditions during all runs. Furthermore, drying in between the runs is observed. With investigating the time-series presented in Figure 4-15B a few important aspects become apparent. The saltation intensity signal shows an intermittent response at the start of the experiment. This trend is reflected in the grain counts that keeps reaching zero alternated with instances of more intense saltation. This signal is associated with peaks and troughs in the wind speed. The intermittent signal continues until some minutes past 14h00. Later, a continuous saltation intensity signal develops. Some minutes past 14:30, an increase in average wind speed is observed, this increase in wind speed is however not reflected in the saltation intensity signal that counts similar grains as before the wind speed increment.

Interestingly, the shift from an intermittent to continuous signal was observed at a point in time when recorded wind speeds were not higher for the continuous signal compared to the intermittent signal. Wind speeds as recorded around 13h45 lie above 10 m/s and correspond to an intermittent signal. Where some minutes past 14h wind speeds are lower (<10 m/s) during a continuous signal (at the start of an increasing wind speed signal). Suggesting that moisture controlled the saltation intensity up to some minutes past 14h, making for an intermittent signal where only occasionally grains are released. When sufficient drying took place the saltation signal shifted from intermittent to continuous for a similar (or even slightly smaller) wind speed. The shift from intermittent to continuous saltation was observed during moisture conditions of 11.5 % at the threshold zone which was located 14m in front of the SalDecS. From the visual transport observations as shown in Figure (4-15A) the static transport threshold zone lies close to the SalDecS (In between 2 and 10m) during the intermittent signal, while during continuous transport conditions the threshold zone shifts up-wind (14 to >18 m in front of the SalDecS).

The results reflect the proposed and interlinked nature of a threshold that is controlled by both wind-speed/gustiness and moisture. During an intermittent saltation signal, short-term (one minute) fluctuations in wind speed show some visual correlation with saltation activity. With continued surface drying, the saltation signal developed to a more continuous response for the same wind speed and the short-term fluctuations in wind speed are less pronounced in the saltation signal.

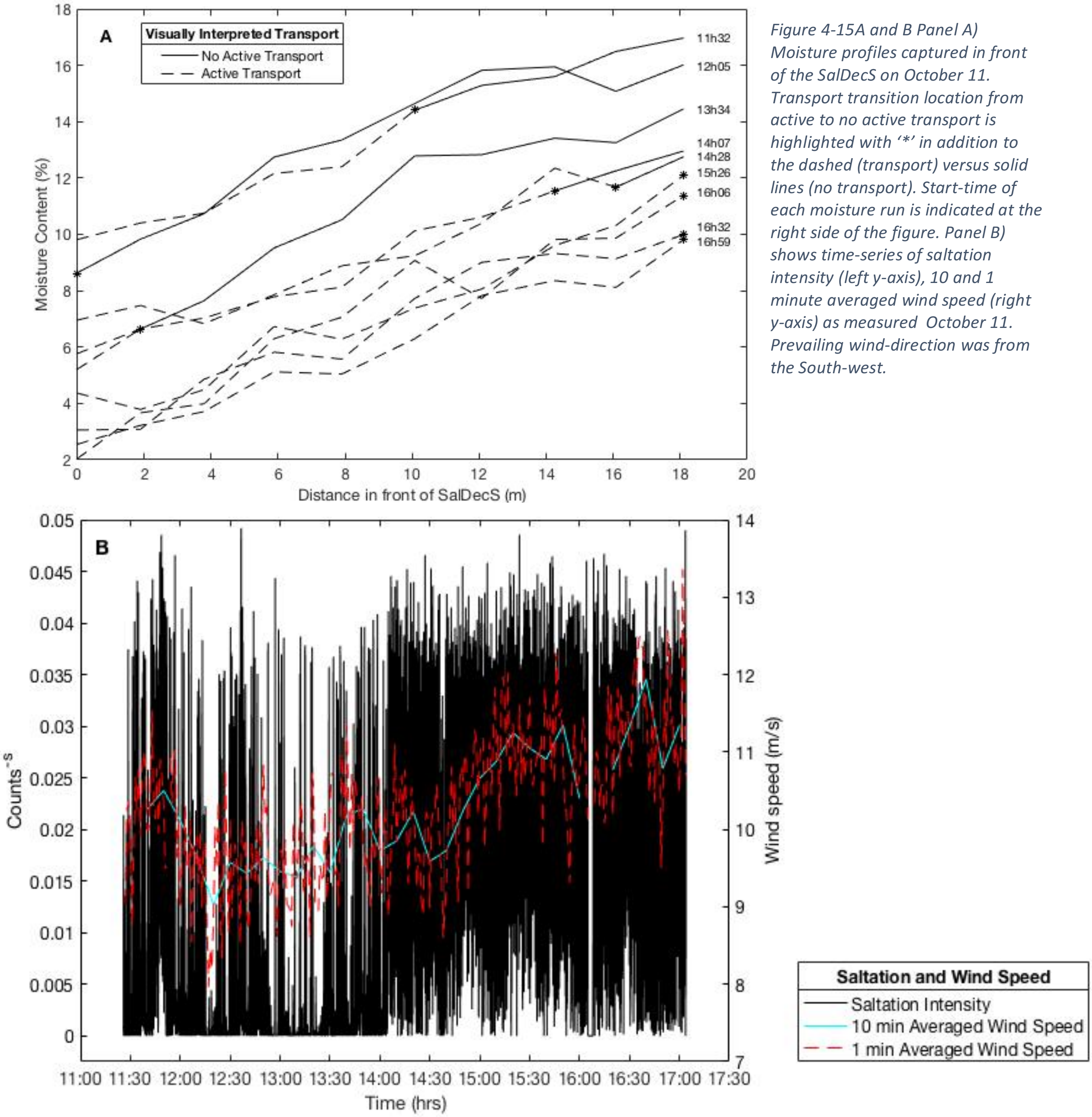

Figure 4-15A and B Panel A) Moisture profiles captured in front of the SalDecS on October 11. Transport transition location from active to no active transport is highlighted with '' in addition to the dashed (transport) versus solid lines (no transport). Start-time of each moisture run is indicated at the right side of the figure. Panel B) shows time-series of saltation intensity (left y-axis), 10 and 1 minute averaged wind speed (right y-axis) as measured October 11. Prevailing wind-direction was from the South-west.*

4.7 Potential Beach Available for Aeolian Entrainment

The spatial variability of surface moisture as captured over the course of the field-campaign is distributed in threshold classes as proposed by Delgado-Fernandez (2011) and Sarre (1984). The classes reflect the proportion of the beach where entrainment theoretically is prohibited due to moisture conditions of ≥ 10% and ≥ 14% respectively (Figure 4-16).

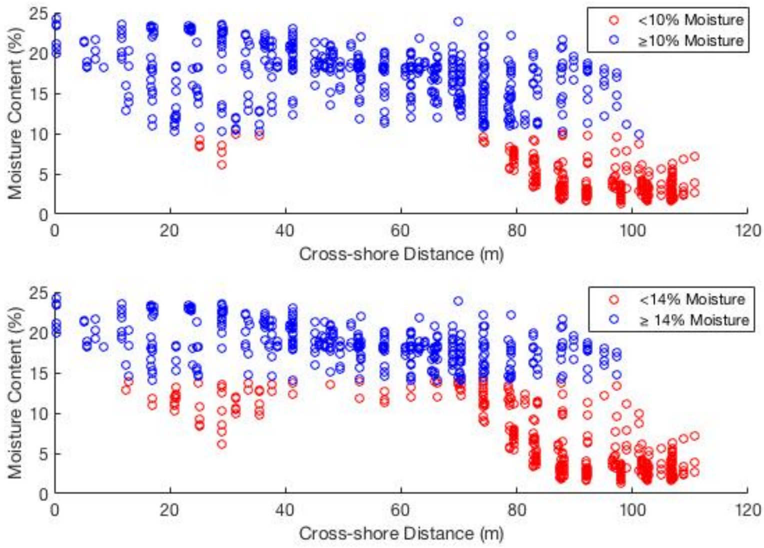

Figure 4-16 Moisture as captured during the entire field-campaign along the groundwater well transect. Spatial distribution of erodible beach area (red) with thresholds at 10% (upper panel) and at 14% (lower panel).

Both choices of moisture threshold (< 10% and < 14% moisture) result in very different maximum erodible beach lengths. The mid-beach is not available for entrainment with a decision of 10% moisture as limit from where transport might happen. However, if entrainment is allowed up to 14% moisture the mid-beach sometimes becomes available for transport. If these conditions coincide with dry conditions near the shore during low-water, the area of the beach that becomes available for transport is drastically increased. These results suggest that small changes (1-4%) in threshold condition can strongly alter the available fetch distance.

These results are incorporated in the following figure (Figure 4-17) that allows comparison of the maximum fetch distance during the field-campaign and the moisture dependent critical fetch distance based on Delgado-Fernandez (2011). The figure reveals that on the Egmond aan Zee beach the critical fetch distance can only be reached during relatively low wind speeds (just above the threshold of motion) or during highly oblique winds but certainly not during high wind speeds that are directed (close to) shore-normal.

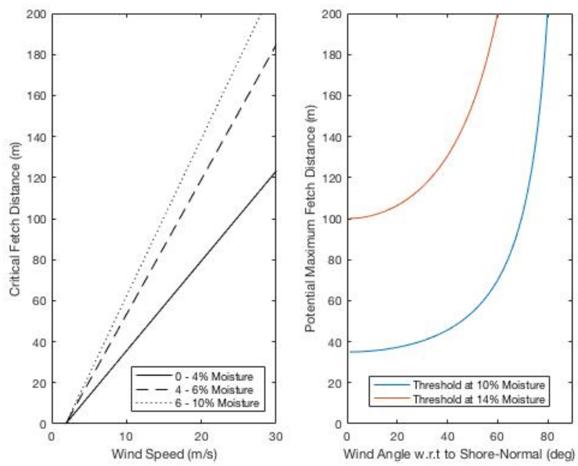

Figure 4-17 Critical fetch distance and potential maximum fetch distance.

5. Discussion

Findings on Temporal and Spatial Surface Moisture Variability

Coastal geomorphologists have long struggled to match long-term model predictions of fore-dune evolution to observed changes in foredune geometry (Davidson-Arnott and Law, 1990; Nordstrom and Jackson, 1992; Arens, 1996; Bauer et al., 2009; Schmutz and Namikas 2018). A number of processes have been accounted to the mismatch, including changes of the wind field as it travels from the sea over the beach to the foredune (Bauer et al., 2009). Furthermore, the time and distance that is required for the saltation cloud to develop to equilibrium transport conditions is known to complicate transport events. This discrepancy may be (partly) overcome by including the fetch effect as proposed by Delgado-Fernandez (2010) that uses a different set of equations as the critical fetch distance is not reached. Observations on temporal and spatial moisture variation may help fine-tune these types of models that account for spatial moisture variability.

Cross-shore, hourly measurements over the course of one month serve to illustrate the variability of the surface moisture content on a beach near Egmond aan Zee. The high degree in variation is associated with the large number of controlling factors that work on different time and spatial scales as was found by some other authors (Zhu, 2007; Namikas *et al.*, 2010 and others). The semi-diurnal tidal influence on groundwater oscillations showed to strongly influence moisture fluctuations at the surface of the beach. Elevation of the phreatic surface showed to generally increase landward as was found on many other beaches (Turner et al., 1995; Raubenheimer *et al.,* 1999; Horn, 2002). Furthermore, tidal induced oscillations of which the amplitude decreases in the landward direction were observed (Lanyon *et al.,* 1982). High-water phase-lag was present and showed to increase in the landward direction.

The surface moisture variability as was found on this beach over the course of the highly energetic field-campaign is described as follows. Generally, a cross-shore gradient in the surface moisture distribution was present, with saturated conditions up to some distance away from the waterline and landward decreasing moisture conditions, up to dry conditions near the dune toe. This distribution changes with the tides. During low-water the gradient is less pronounced, and variation in moisture content is distributed over the entire intertidal beach. During high-tide, the gradient becomes larger and a rapid decrease in moisture content from the waterline to the dune-toe was observed. On instances where the slope of the phreatic surface is equal to the slope of the beach, uniform moisture conditions on the intertidal beach are present. These instances are related to the development of a flat beach profile associated with the morphological redistribution of sand. During these morphological conditions, uniform drying was observed with a falling watertable. Potentially large aeolian transport may occur on these instances, if a threshold of motion is exceeded, it is exceeded on the entire mid-beach.

Saturated conditions are present in an area defined by the seaward edge of the non-inundated beach up to some distance landward. The seaward edge of this zone shifts with the inundation level of the beach due to the tidal elevation and the maximum wave run-up limit, slope, morphology wave height and set-up are important controlling factors. The landward extend of the saturated zone is altered mostly by the depth of the groundwater table and the presence and thickness of the capillary fringe that causes saturated conditions with a groundwater table up to 0.20m meter below the surface on the Egmond aan Zee beach. The thickness of the capillary fringe may vary with the seasons and on other beaches depending on the present grainsize (Medina et al., 1994).

The zone of the beach that is characterised neither by saturated or dry conditions showed to vary with oscillations in the groundwater table. During a falling groundwater table, associated with a falling tide, surface drying over the entire non-inundated beach was observed. The surface wetness for any groundwater depth below the beach surface can be predicted with the Soil Water Characteristic Curve (SWCC), that was on this beach fitted to observations. The distance from the phreatic surface to the surface of the beach showed to be a key factor that determines the surface wetness. Therefore, the topography of the intertidal beach (that showed next to cross-shore spatio-temporal variability also alongshore variability) is important in altering the surface moisture distribution.

In contrast to other studies (Zhu, 2007; Namikas, 2010; Schmutz and Namikas, 2018), evaporation and rainfall showed to be of second order importance in controlling the surface moisture distribution compared to the depth of the groundwater table. Eventhough temperatures where measured at maximum 25 deg C during October 16. The small relative importance of evaporation can be explained by the small incoming solar radiation during October at a latitude of 52 deg N. Also, the hysteresis effect due to a falling and rising groundwater table did not show any important influence on the surface moisture system as proposed by Schmutz and Namikas (2013). Furthermore, the transient nature of water flow in unsaturated sediment (Schmutz and Namikas, 2013) could not be recognized in the field observations. These processes become more important in sediments where capillary forces are greater compared to other flow driving mechanisms, on beaches this would be mostly determined by the grainsize mean diameter.

The topography and morphological evolution of the beach are altered by imposed wave conditions (Hoefel and Elgar, 2003). An elevated groundwater table and decreased beach surface elevation with the occurrence of storm surges made for exceptionally wet conditions over the intertidal beach. Shifting of the saturated zone after a storm surge is associated with the migration speed of a seepage-face exit-point, landward of this point the SWCC best describes the drying. High wind speeds associated with periods around storm surges hold potentially large aeolian transport input based on imposed wind shear. However, observations of surface moisture during and after a storm surge reveal a mostly saturated mid-beach that reduces the potential beach area available for aeolian transport and partly or totally closes the aeolian system.

Evolution of the beach morphology after fair-weather conditions (development and migration of an intertidal bar was observed) showed to influence the surface moisture distribution. More specific, the intertidal bar showed fast and pronounced drying compared to slow drying in the associated trough. However, relevance in aeolian sediment supply to the foredune during conditions of pronounced transport from the bar seems limited, because aeolian depocenters associated with the wet troughs are present as was found by (Oblinger and Anthony, 2008). However, observations during the field campaign also revealed aeolian transport over the wet trough onto the mid-beach during high wind speeds.

Next to the influence of the discussed controlling environmental factors, also influence of the aeolian transport system on moisture content should be noted. Aeolian bedforms introduce dry sand to the beach surface (since grains dry significantly during transport) while erosion of the beach reveals ‘new’ wet sand to the system that might be harder to be entrained. Thus, even if environmental factors as meteorological conditions and groundwater levels remain constant over space and time, variability in surface moisture may occur in response to aeolian transport (Delgado - Fernandez, 2011).

Findings on Moisture Dependent Entrainment Thresholds

Observations of entrainment thresholds revealed an increase in threshold wind-speed with surface moisture content. The relation is characterised by a large amount of scatter in the data and a clear relation between depth-integrated moisture content and threshold wind speed could not be established. Pronounced and rapid surface drying and stripping could explain the large amount of scatter in the threshold observations (Davidson-Arnott *et al.*, 2008; Bauer *et al.,* 2009). Because moisture observations integrated over 0.02m do not reflect true surface wetness on which the wind shear acts. This notion might also explain the observed transport from (near) saturated sediments, where only the very surface of the sediment (1-2 mm) dries sufficient to subsequently become entrained. Rapid surface drying together with the presence of unsteady winds further complicate the establishment of a relation between moisture content and threshold wind speed.

The wet critical shear velocity calculations based on the Bagnold (1936) equations corrected for moisture content by the Belly (1962) equation. The curve explains some of the observations but is far from indicative, especially in the region of low threshold wind speeds over-prediction of the threshold by model is present. The moisture corrections seem reasonably in line with field observations in the moisture range from 8 - 14% moisture. These findings are in line with remarks on the moisture corrected critical shear of Sarre (1984). In contrast, predictions based on dry (uncorrected) critical shear are in line with field-observations.

Observations of saltation intensity and moisture profiles in front of the detection systems revealed a shift from moisture controlled intermittent transport to wind controlled continuous transport as was found by some other authors (Wiggs, Baird and Atherton, 2003). This shift was observed when the beach dried past 10% moisture during a wind speed of around 10 m/s. From the saltation intensity observations became apparent that rapid surface drying is less important during continuous transport conditions. This implies that efforts on finding a temporal and spatially varying threshold hold zone are not futile given the complexities of an unsteady windfield and large temporally varying moisture gradients at the very surface of the beach. The determination of a temporally and spatially shifting threshold zone around 10% moisture could help define an area from where landward continuous transport is potentially possible. The shifting of the 10% contour could denote the point in space and time from where-on landward continuous transport can simulated.

The spatial and temporal surface moisture variation as presented in this study were observed during the stormy season in the Netherlands, reflected by the two surges that occurred during the field period. It should be noted that the moisture distribution is expected to be dryer during summer and spring. These seasons are less effected by large low-pressure systems that cause most of the energetic sea-state conditions. From the surface moisture - watertable plot (Figure 5-8) became apparent that the proposed entrainment thresholds (at 10% moisture) are associated with a groundwater table depth of 0.35m. It seems realistic that part of the beach with a groundwater table depth greater than 0.35 becomes larger during low-energetic seasons, since elevated groundwater tables after the storms were found to remain present days after the storms had passed. Subsequently, the time during which the beach area is potentially available for transport based on surface moisture conditions increases with the lack of storms.

It is important to note that the storms that produce transport (based on wind shear) might also shut-down the aeolian system due to the presence of a seepage face. In this sense, Southwestern storms in the Netherlands are more likely to produce transport that reaches the fore-dune compared to North-western storms since surges are more likely during the latter wind direction. During shore-normal western storms surges are not likely, during these conditions the fetch effect becomes important in limiting transport. During these conditions, high transport rates associated with equilibrium transport during strong winds are not reached. In light of these remarks transport during light wind events (around 5-6 m/s winds) could be important in delivering significant amounts of sand volume to the dunes, also because light wind events are more likely to happen than stronger storms. Furthermore, during alongshore winds equilibrium transport is very likely even during strong winds due an unlimited fetch distance but transported sand will not attribute to dune growth in this case.

Decision in threshold condition is important in determining how much beach becomes available for transport. Small changes (1-4%) in threshold condition may results in large differences in beach that becomes potentially available. A change in threshold moisture content of 4% (from 10 to 14%) can result in a change of available fetch distance of some 65m (from maximum available fetch of 35m with a 10% threshold to maximum available fetch of 100m with a 14% threshold) (figure 4-16). This change can be caused by a small groundwater table variation of 0.05m (from 0.32m to 0.27).

6. Conclusions

- The tidal cycle influences the surface moisture content by altering the groundwater table depth below the surface of the beach. Oscillations of the groundwater table follow the same frequency as the tides, but undergo some changes as the signal propagates into the beach. The changes include amplitudal decrease, phase-lag increase and presence of overheight, these deviations from the tidal signal become stronger landward. The variation of surface moisture content is linked to the groundwater table by a fitted Soil Water Characteristic Curve. This function relates the surface moisture content and depth of the watertable below the surface of the beach. By highlighting moisture data based on meteorological conditions that prevailed during the collection, factors as rain and evaporation showed to be of second order importance in altering the surface moisture content since no specific organization of the data above or below the fitted curve was observed.
- Temporally, the surface moisture content varied over both a semi-diurnal and fortnightly scale associated with the half-daily and spring-neap tidal cycles. The semi-diurnal scale mostly showed variation with inundation of the beach. The spring-neap cycle was less pronounced in altering the moisture conditions. However, the increased tidal range during spring-tide made for larger moisture variations, during neap tide the opposite was observed, with smaller variations and a dryer upper-beach.
- Spatially, the surface moisture content showed a general gradient that increased moving seaward. This gradient was less pronounced during low-water and more pronounced during high-water. Interruptions of the gradient are associated with the presence of an intertidal sandbar.
- The beach morphology (presence of bars and troughs) influences the surface moisture content since the groundwater table does not follow details of the morphology but is a rather smooth surface below the beach. Elevated parts of the beach bear dryer conditions and lower situated areas hold wetter conditions. The morphology showed to be an important factor in altering the alongshore moisture variability.
- Surface moisture conditions after a storm-surge are characterised by the presence of a seepage face. The seaward migration of the exit-point lags behind the falling tide, the groundwater table is therefore decoupled from the tidal signal. Potential aeolian transport during these conditions is limited, because the seepage face prohibits sand entrainment and closes the aeolian system seaward of the exit-point.
- Visual observations on wind and moisture dependent entrainment thresholds showed that the threshold increases with wetter moisture conditions. The threshold seems to be greatly influenced by the rate of drying of the very surface of the sediment.
- Observations on saltation intensity and up-wind sampled moisture profiles showed a clear transition from intermittent to continuous transport around 11.5% moisture associated with drying of the windward side of the beach.
- The effect of spatial and temporal moisture variability on windblown sand transport on wave dominated beaches could be reflected in models by simulating a moisture dependent fetch effect. The shifting transition zone of intermittent to continuous transport might be a useful indicator that dissects the use of different transport equations. This region should however not be confused with the transition of non-equilibrium to equilibrium transport (and the use of

subsequent equations). Continuous transport might as well be still developing towards equilibrium with the wind field, this is especially likely during high wind speeds.

7. Future Research

Instead of visually assessing if transport happens near the threshold of motion, the saltation detection systems placed near the threshold zone could be deployed for this purpose. Future observations using a terrestrial laser scanner as used by (Smit *et al.,* 2017) that is able to capture the moisture content of the very beach surface at a high frequency with a large continuous spatial coverage during transport events might help shed light on entrainment thresholds. Furthermore, investigating how fast drying of the upper few millimetres of the beach happens for different wind speeds during aeolian activity might shed light on the process of surface drying and subsequent sand stripping.

8. Acknowledgements

I would like to thank my co-students and colleagues in the field; Corinne Bohm, Job van Beem and Jorn Bosma. They all provided very helpful hands and important insights during the fieldwork, not to mention the good times we had on the beach! Furthermore, I would like to thank my supervisors Jasper Donker and Gerben Reussink for their insights both in the field and during the period of processing and analysing the data. Furthermore, feedback by both supervisors on the first draft version of this thesis proved to be very helpful!

9. References

Arens, S. M. (1996). Rates of aeolian transport on a beach in a temperate humid climate. *Geomorphology*, *17*(1-3), 3-18.

Atherton, R. J., Baird, A. J., & Wiggs, G. F. (2001). Inter-tidal dynamics of surface moisture content on a meso-tidal beach. *Journal of Coastal Research*, 482-489.

Bagnold, R. A. (1936). The movement of desert sand. *Proc. R. Soc. Lond. A*, *157*(892), 594-620.

Bauer, B. O., & Davidson-Arnott, R. G. (2003). A general framework for modeling sediment supply to coastal dunes including wind angle, beach geometry, and fetch effects. *Geomorphology*, *49*(1), 89-108.

Bauer, B. O., Davidson-Arnott, R. G. D., Hesp, P. A., Namikas, S. L., Ollerhead, J., & Walker, I. J. (2009). Aeolian sediment transport on a beach: Surface moisture, wind fetch, and mean transport. *Geomorphology*, *105*(1), 106-116.

Belly, P. Y. (1962). *Sand movement by wind* (No. S-72-I-7). CALIFORNIA UNIV BERKELEY INST OF ENGINEERING RESEARCH.

Blott, S. J., & Pye, K. (2001). GRADISTAT: a grain size distribution and statistics package for the analysis of unconsolidated sediments. *Earth surface processes and Landforms*, *26*(11), 1237-1248.

Blott, S. J. (2010). GRADISTAT ver. 8.0: A grain size distribution and statistics package for the analysis of unconsolidated sediments by sieving or laser granulometer. *Kenneth Pye Associates Ltd, UK (www. kpal. co. uk/gradistat. html)*.

Cornelis, W. M., & Gabriels, D. (2003). The effect of surface moisture on the entrainment of dune sand by wind: an evaluation of selected models. *Sedimentology*, *50*(4), 771-790.

Davidson-Arnott, R. G., & Law, M. N. (1990). Seasonal patterns and controls on sediment supply to coastal foredunes, Long Point, Lake Erie. *Coastal dunes: form and process*, *2*, 177.

Davidson-Arnott, R. G., & Law, M. N. (1996). Measurement and prediction of long-term sediment supply to coastal foredunes. *Journal of Coastal Research*, 654-663.

Davidson-Arnott, R. G., MacQuarrie, K., & Aagaard, T. (2005). The effect of wind gusts, moisture content and fetch length on sand transport on a beach. *Geomorphology*, *68*(1), 115-129.

Davidson-Arnott, R. G., Yang, Y., Ollerhead, J., Hesp, P. A., & Walker, I. J. (2008). The effects of surface moisture on aeolian sediment transport threshold and mass flux on a beach. *Earth Surface Processes and Landforms*, *33*(1), 55-74.

Darke, I., & Neuman, C. M. (2008). Field study of beach water content as a guide to wind erosion potential. *Journal of Coastal Research*, 1200-1208.

Delgado-Fernandez, I. (2010). A review of the application of the fetch effect to modelling sand supply to coastal foredunes. *Aeolian Research*, *2*(2-3), 61-70.

Delgado-Fernandez, I., & Davidson-Arnott, R. (2011). Meso-scale aeolian sediment input to coastal dunes: The nature of aeolian transport events. *Geomorphology*, *126*(1-2), 217-232.

Delta-T Devices, 2005. User manual for the Moisture Meter type HH2, version 4.0. Delta-T Devices, Burwell, Cambridge, England.

van Duin, M. J. P., Wiersma, N. R., Walstra, D. J. R., Van Rijn, L. C., & Stive, M. J. F. (2004). Nourishing the shoreface: observations and hindcasting of the Egmond case, The Netherlands. *Coastal Engineering*, *51*(8), 813-837.

Everard, M., Jones, L., & Watts, B. (2010). Have we neglected the societal importance of sand dunes? An ecosystem services perspective. *Aquatic Conservation: Marine and Freshwater Ecosystems*, *20*(4), 476-487.

Edwards, B. L., & Namikas, S. L. (2009). Small-scale variability in surface moisture on a fine-grained beach: implications for modeling aeolian transport. *Earth Surface Processes and Landforms*, *34*(10), 1333-1338.

Ellis, J. T., & Sherman, D. J. (2013). 11.6 Fundamentals of Aeolian Sediment Transport: Wind-Blown Sand.

Fitts, C. R. (2002). *Groundwater science*. Academic press.

Gourlay, M. R. (1992). Wave set-up, wave run-up and beach water table: Interaction between surf zone hydraulics and groundwater hydraulics. *Coastal engineering*, *17*(1-2), 93-144.

van Genuchten, M. T. (1980). A closed-form equation for predicting the hydraulic conductivity of unsaturated soils 1. *Soil science society of America journal*, *44*(5), 892-898.

Hagen, G. (1863). *Handbuch der Wasserbaukunst: 3: Seeufer und Hafen-Bau*. Ernst & Korn.

Hillel, D. (1998). *Environmental soil physics: Fundamentals, applications, and environmental considerations*. Elsevier.

Horn, D. P. (2002). Beach groundwater dynamics. *Geomorphology*, *48*(1), 121-146.

Hoefel, F., & Elgar, S. (2003). Wave-induced sediment transport and sandbar migration. *Science*, *299*(5614), 1885-1887.

Jackson, N. L., & Nordstrom, K. F. (1997). Effects of time-dependent moisture content of surface sediments on aeolian transport rates across a beach, Wildwood, New Jersey, USA. *Earth Surface Processes and Landforms: The Journal of the British Geomorphological Group*, *22*(7), 611-621.

Kadib, A. A. (1965). *A function for sand movement by wind* (No. HEL-2-12). CALIFORNIA UNIV BERKELEY HYDRAULIC ENGINEERING LAB.

Lettau, K. (1978). Experimental and micrometeorological field studies of dune migration. *Exploring in the World's driest climate*, 110-147.

Li, L., Barry, D. A., & Pattiaratchi, C. B. (1997). Numerical modelling of tide-induced beach water table fluctuations. *Coastal Engineering*, *30*(1-2), 105-123.

Nayar, K. G., Panchanathan, D., McKinley, G. H., & Lienhard, J. H. (2014). Surface tension of seawater. *Journal of Physical and Chemical Reference Data*, *43*(4), 043103.

Namikas, S. L., & Sherman, D. J. (1995). A review of the effects of surface moisture content on aeolian sand transport. In *Desert aeolian processes* (pp. 269-293). Springer, Dordrecht.

Namikas, S. L., Edwards, B. L., Bitton, M. C. A., Booth, J. L., & Zhu, Y. (2010). Temporal and spatial variabilities in the surface moisture content of a fine-grained beach. *Geomorphology*, *114*(3), 303-310.

Nickling, W. G., & Ecclestone, M. (1981). The effects of soluble salts on the threshold shear velocity of fine sand. *Sedimentology*, *28*(4), 505-510.

Nickling, W. G. (1984). The stabilizing role of bonding agents on the entrainment of sediment by wind. *Sedimentology*, *31*(1), 111-117.

Nield, J. M., Wiggs, G. F., & Squirrell, R. S. (2011). Aeolian sand strip mobility and protodune development on a drying beach: examining surface moisture and surface roughness patterns measured by terrestrial laser scanning. *Earth Surface Processes and Landforms*, *36*(4), 513-522.

Nielsen, P. (1990). Tidal dynamics of the water table in beaches. *Water Resources Research*, *26*(9), 2127-2134.

Nielsen, P., & Kang, H. Y. (1996, January). Groundwater dynamics in beaches and coastal barriers. In *Coastal Dynamics' 95* (pp. 521-532).

Nordstrom, K. F., & Jackson, N. L. (1992). Effect of source width and tidal elevation changes on aeolian transport on an estuarine beach. *Sedimentology*, *39*(5), 769-778.

McKenna-Neuman, C., & Nickling, W. G. (1989). A theoretical and wind tunnel investigation of the effect of capillary water on the entrainment of sediment by wind. *Canadian Journal of Soil Science*, *69*(1), 79-96.

McKenna Neuman, C., & Langston, G. (2006). Measurement of water content as a control of particle entrainment by wind. *Earth Surface Processes and Landforms*, *31*(3), 303-317.

Lanyon, J. A., Eliot, I. G., & Clarke, D. J. (1982). Groundwater-level variation during semidiurnal spring tidal cycles on a sandy beach. *Marine and Freshwater Research*, *33*(3), 377-400.

Oblinger, A., & Anthony, E. J. (2008). Surface moisture variations on a multibarred macrotidal beach: implications for aeolian sand transport. *Journal of Coastal Research*, 1194-1199.

Pollock, L. W., & Hummon, W. D. (1971). Cyclic changes in interstitial water content, atmospheric exposure, and temperature in a marine beach. *Limnology and Oceanography*, *16*(3), 522-535.

Poortinga, A., Keijsers, J. G. S., Visser, S. M., Riksen, M. J. P. M., & Baas, A. C. W. (2015). Temporal and spatial variability in event scale aeolian transport on Ameland, The Netherlands. *GeoResJ*, *5*, 23-35.

Pugh, D. T. (1996). *Tides, surges and mean sea-level (reprinted with corrections)*. John Wiley & Sons Ltd.

Raubenheimer, B., Guza, R. T., & Elgar, S. (1999). Tidal water table fluctuations in a sandy ocean beach. *Water Resources Research*, *35*(8), 2313-2320.

Sánchez-Úbeda, J. P., Calvache, M. L., Duque, C., & López-Chicano, M. (2016). Filtering methods in tidal-affected groundwater head measurements: Application of harmonic analysis and continuous wavelet transform. *Advances in Water Resources*, *97*, 52-72.

Sarre, R.D. 1984: Sand movement from the intertidal zone and within coastal dune systems by aeolian processes. University of Oxford, unpublished PhD thesis.

Schmutz, P. P., & Namikas, S. L. (2011). Utility of the Delta-T Theta Probe for obtaining surface moisture measurements from beaches. *Journal of Coastal Research*, *27*(3), 478-484

Schmutz, P. P., & Namikas, S. L. (2013). Measurement and modeling of moisture content above an oscillating water table: implications for beach surface moisture dynamics. *Earth Surface Processes and Landforms*, *38*(11), 1317-1325.

Schmutz, P. P., & Namikas, S. L. (2018). Measurement and modeling of the spatiotemporal dynamics of beach surface moisture content. *Aeolian Research*, *34*, 35-48.

Sherman, D. J. (1990a). 'Discussion: Evaluation of aeolian sand transport equations using intertidal zone measurements, Saunton Sands, England'. *Sedimentology*, 37, 385–388.

Smit, Y., Ruessink, G., Brakenhoff, L. B., & Donker, J. J. (2017). Measuring spatial and temporal variation in surface moisture on a coastal beach with a near-infrared terrestrial laser scanner. *Aeolian Research*.

Sokolów, N.A. (1894) Die Du¨nen: Bildung. Entwickelung und innerer Bau (translated from the Russian by A. Arzruni). Springer, Berlin, pp. 298.

Tsegaye, T. D., Tadesse, W., Coleman, T. L., Jackson, T. J., & Tewolde, H. (2004). Calibration and modification of impedance probe for near surface soil moisture measurements. *Canadian journal of soil science*, *84*(2), 237-243.

Turner, I. L., Coates, B. P., & Acworth, R. I. (1997). Tides, waves and the super-elevation of groundwater at the coast. *Journal of Coastal Research*, 46-60.

Wiggs, G. F. S., Baird, A. J., & Atherton, R. J. (2004). The dynamic effects of moisture on the entrainment and transport of sand by wind. *Geomorphology*, *59*(1), 13-30.

de Winter, W., van Dam, D. B., Delbecque, N., Verdoodt, A., Ruessink, B. G., & Sterk, G. (2018). Measuring high spatiotemporal variability in saltation intensity using a low-cost Saltation Detection System: Wind tunnel and field experiments. *Aeolian Research*.

de Winter, R. C., Gongriep, F., & Ruessink, B. G. (2015). Observations and modelling of alongshore variability in dune erosion at Egmond aan Zee, the Netherlands. *Coastal Engineering*, *99*, 167-175.

Wolfe, S. A., & Nickling, W. G. (1993). The protective role of sparse vegetation in wind erosion. *Progress in physical geography*, *17*(1), 50-68.

Yang, Y., & Davidson-Arnott, R. G. (2005). Rapid measurement of surface moisture content on a beach. *Journal of Coastal Research*, 447-452.

Zhu, Y. (2007). *Modeling spatial and temporal variations of surface moisture content and groundwater table fluctuations on a fine-grained beach, padre island, texas* (Doctoral dissertation).